PERGAMON

International Journal of Solids and Structures 37 (2000) 4655–4690

INTERNATIONAL JOURNAL OF SOLIDS and STRUCTURES

www.elsevier.com/locate/ijsolstr

On thermal buckling of patched beam-plates

A.M. Karlsson, W.J. Bottega*

Department of Mechanical and Aerospace Engineering, Rutgers University, 98 Brett Road, Piscataway, NJ 08854-8058 USA

Received 10 October 1998; in revised form 2 April 1999

Abstract

The behavior of uniformly heated plates is considered for the situation where a patch is adhered over a region of the structure. A variational formulation results in a self-consistent set of equations and conditions, which governs the response of the system. The nonlinear problems are solved analytically, yielding exact results within the context of the mathematical model employed. A stability criterion is established for the class of problems considered, based on the second variation of the potential energy of the composite structure, and issues of stability are assessed in this context. Three non-dimensional parameters that characterize the response of the structure are identified. These are a 'loading parameter', a 'critical temperature' and a 'critical membrane force'. Results of numerical simulations are presented for various loading and support conditions, patch lengths, and mechanical properties of the components. It is seen that bifurcation buckling, 'asymptotic buckling', and 'sling-shot buckling' are all possible scenarios for the class of structures of interest.

Keywords: Beam; Bifurcation; Bimaterial; Buckling; Composite; Laminate; Patched structures; Plate; Post-buckling; Sling-shot buckling; Snap-through; Stability; Temperature; Thermal buckling

1. Introduction

Many thin structures consist of a primary component to which a secondary component is adhered, thus forming a 'composite structure'. Examples of such structures range from a patch adhered to a damaged structure to prevent further crack-propagation, to thin films on electronic substrates. In particular, the use of repair patches on aircraft structures has received increased attention in recent years. Examples of related work pertaining to patched structures may be found in the papers by Roderick (1980), Sih and Hong (1989), Baker (1993), Bottega (1995), Bottega and Loia (1996, 1997), Bottega and Karlsson (1999), and Karlsson and Bottega (1999a, 1999b). Though 'patching' may be an

* Corresponding author Tel.: +001-732-445-4282; Fax: +001-732-445-5313.
E-mail address: bottega@rci.rutgers.edu (W.J. Bottega).

0020-7683/00/$ - see front matter
PII: S0020-7683(99)00134-1

effective way to repair a cracked structure, there are several sources which can eliminate the efficiency of the repair, such as debonding of the patch, and complications arising from mismatch of thermal properties between the patch and the base structure. It was seen in Bottega (1995), Bottega and Loia (1996, 1997), Bottega and Karlsson (1999) and Karlsson and Bottega (1999a, 1999b) that the debonding scenario may vary significantly depending upon the boundary conditions, loading conditions and structural configurations. In work done by Naboulsi and Mall (1997) and by Lena et al. (1998), thermal loading was considered, though the emphasis was on the residual thermal stresses, which are indeed of major concern. However, a change in temperature may also induce instability of a thin structure, such as bifurcation buckling, snap-through buckling, or 'just' unacceptable large out-of-plane deflections of the structure. To the knowledge of the authors' of the present study, no studies on thermal buckling of patched structures are found in the open literature. However, investigations have been concerned with the related problem of thermally induced buckling of laminates, as discussed below.

Thermoelastic buckling of beam-plates and plates has long been of vivid interest to researchers. Perfectly isotropic beams and plates, which are fixed from motion in their plane, are found to exhibit bifurcation buckling at a critical temperature when they are exposed to a homogeneous temperature field (i.e., the plate will remain flat during increasing temperature until a critical temperature is reached, at which point the magnitude of transverse deflection becomes indeterminant (see, for example, Boley (1997)). For the case of an isotropic beam or plate with an imperfection, the structure will not exhibit bifurcation buckling. Instead, the structure will exhibit a transverse deflection immediately upon subjection to a temperature field, with magnitude and direction depending on the nature of the imperfection. At elevated temperatures the deflections become very large, to the extent that the structure is, in effect, unusable after a certain temperature. In addition, other deformation scenarios are possible for different degrees of anisotropy of the beam or plate. For certain non-isotropic structures, such as a bilaminate, the structure may exhibit snap-through buckling (i.e., the structure moves dynamically from one configuration to another) when subjected to critical thermal loads. A now classic work regarding thermally induced snap-through buckling was published by Timoshenko (1925), where the response of a bilayer strip/beam to thermal loading was examined. Bending and snap-through buckling were found to occur upon heating to an appropriate level, while snap-back was seen to occur as well when the system was appropriately cooled. Wahl (1944) examined the 'Valverde' thermostat, consisting of three pre-stressed strips. It was shown that, upon heating, the strips buckle in a snap-through mode. Snap-back occurred during cooling. In the papers by Wittrick (1953) and Wittrick et al. (1953) the thermoelastic stability of a shallow bilayered spherical cap was considered. Snap-through behavior was seen to occur when the temperature was sufficiently increased for certain structures, as well as snap-back when the temperature was lowered to a critical level. For the structures considered by Timoshenko (1925), Wahl (1944), Wittrick (1953) and Wittrick et al. (1953) snap-through occurred at higher temperatures than snap-back.

Since these early studies, a number of investigations have been performed concerning buckling and post-buckling of laminated structures (beams and plates) under thermal loads. Surveys of such studies can be found in the reviews by Tauchert (1991) and by Noor and Burton (1992). The former survey is focused on the structural response of plates due to a range of loading conditions, including temperature loading, while the latter deals with the response of composite plates in a temperature field, in general, and includes issues of instability. The discussions by Tauchert (1991) and by Noor and Burton (1992) will not be repeated herein, but pertinent studies include work done by Huang and Tauchert (1988), Hamamoto and Hyer (1987), Gauss and Antman (1984), Noor and Peters (1992), and Noor et al. (1993). Since the surveys by Tauchert (1991) and Noor and Burton (1992), several new studies have been published, for example Librescu and Souza (1993), Singh et al. (1993), Dano and Hyer (1998), and Yin (1998). Librescu and Souza (1993) suggest a model to determine the post-buckling behavior of symmetric laminates with imperfections. Numerical simulations were conducted for selected scenarios

regarding loading, in-plane boundary conditions and the presence of imperfections. In all cases considered therein, all four edges of the rectangular plate are simply supported. Several conclusions are made, and among others, it is suggested that bifurcation buckling does not occur when imperfections are present, but rather large deflections occur after a certain level of the temperature is achieved. Non-symmetric laminates were considered by Singh et al. (1993) and Dano and Hyer (1998). Plates with simply supported edges, which prohibit motion within the plane, were treated by Singh et al. (1993). The results indicate that bifurcation buckling may occur for antisymmetric laminates under some circumstances. Another interesting and important aspect of thermal buckling was considered by Dano and Hyer (1998). This study is concerned with the issue of cooling of an initially flat unsymmetric laminate from an elevated temperature (e.g., the laminate is flat during curing at elevated temperatures). During cooling buckling may occur, thus the laminates are in general not flat once room temperature is reached. The deformation path from curing temperature to the final shape of the structure at room temperature is predicted, and bifurcation buckling is identified during cooling. Snap-through buckling is observed to occur with the subsequent introduction of a transverse load. Yin (1998) investigated the thermomechanical buckling of delaminated composite laminates. In that study, the temperature was allowed to vary arbitrarily through the thickness of the laminate. Modeling the laminate in a one-dimensional fashion, thus considering a beam-plate, enabled the author to solve the stated problem analytically. Among the results discussed is how the bifurcation load changes with the size of the delamination.

In the present study, the response of patched plates subjected to a uniform temperature field is considered for a variety of thermo-mechanical loading and support conditions. The problems are approached from a unified point of view within the theory of calculus of variations. An appropriate thin structure theory is incorporated as the mathematical model for the base structure and the patch individually. In this way a self-consistent model is obtained for the composite structure for the particular system under study. The non-linear formulation lends itself to an exact analytical solution. Due to the non-linearity of the problem, several equilibrium configurations may be found for a given value of the load, hence the stability of the different equilibrium branches of the loading path must be established. In this regard, a stability criterion is established based on the second variation of the potential energy of the system. Stability is assessed along each path, in this context. Intricate results of extensive numerical simulations are presented which elucidate the interesting behavior of the geometrically discontinuous composite structure. Of particular interest are the effects that a mismatch in the coefficients of thermal expansion of the base plate and patch have on the overall response of the heated structure. In addition, the effects that the relative stiffnesses and lengths of the patch have on the behavior of the structure are examined, as are the effects of the thickness to length ratios of the base structure itself.

2. Formulation

Consider a thin flat structure comprised of a base panel of normalized half-span $L \equiv 1$ to which a patch of half-span $L_p \leq 1$ is perfectly adhered. The region where the patch is present is defined as S_1: $x \in [0, L_p]$, as shown in Fig. 1. The coordinate x runs along the upper surface of the base panel and originates at the centerspan of the structure, as shown. Furthermore, the region ahead of the patch (i.e., the region of the composite structure that consists only of the base structure), is defined as S_2: $x \in [L_p, 1]$. We shall be interested in examining the response of the 'composite structure' comprised of the patch and base panel when it is subjected to a uniform temperature increase above some reference temperature. In what follows all length scales are normalized with respect to the dimensional half-span $\bar{L}$ of the undeformed structure and the temperature change, Θ, is normalized with respect to the reference

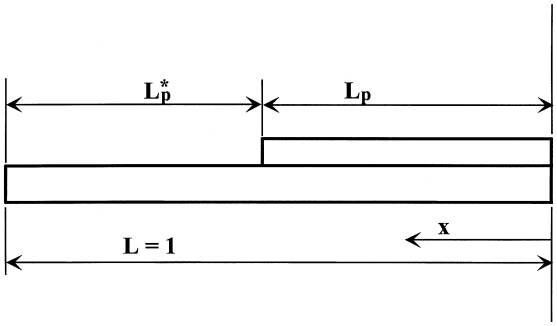

Fig. 1. Geometry of patched beam-plate.

temperature. The interface between the patch and base panel, and its extension (i.e., the upper surface of the base panel), will be used as the reference surface.

The problem may be formulated by paralleling the variational development presented by Bottega (1995), but augmenting the corresponding membrane forces to include the thermal effects in the expression for the membrane energy[1]. Thus, in the expression for the membrane energy in Bottega (1995), $e_i(x)$ is replaced by $e_i(x)-\alpha\Theta$, and $e_p(x)$ is replaced by $e_p(x)-\alpha_p\Theta$,[2] where $e_i(x)$ and $e_p(x)$ are strains, and α and α_p are described in what follows. We remark that since we shall consider the temperature change, Θ, as 'prescribed', its variation shall vanish identically.

The corresponding relations for the normalized (centerline) membrane strains $e_i(x)$ and $e_p(x)$, and the normalized curvature changes $\kappa_i(x)$ and $\kappa_p(x)$, for the base structure and patch in each region are respectively given by

$$e_i = u_i' + \frac{1}{2}w_i'^2, \qquad \kappa_i = w_i'', \qquad x \in S_i, \qquad (i = 1, 2), \tag{1a,b}$$

$$e_p = u_p' + \frac{1}{2}w_p'^2, \qquad \kappa_p = w_p'', \qquad x \in S_1. \tag{1c,d}$$

where $u_i = u_i(x)$ (positive in direction of increasing x) and $w_i = w_i(x)$ (positive downward) respectively correspond to the in-plane and transverse displacements of the centerline of the base panel in region S_i, and $u_p = u_p(x)$ and $w_p = w_p(x)$ correspond to the analogous displacements of the centerline of the patch. In addition, superposed primes indicate total differentiation with respect to x.

The displacements $u_i(x)$ and $u_p(x)$ and the membrane strains $e_i(x)$ and $e_p(x)$ of the substructure centerlines are related to their counterparts at the reference surface, $u_i^*(x)$ and $u_p^*(x)$, and $e_i^*(x)$ and $e_p^*(x)$, by the relations

$$u_i^*(x) = u_i(x) + \frac{1}{2}hw_i', \qquad (i = 1, 2) \tag{2a}$$

[1] A separate functional for 'thermal energies' is not warranted here, as we are considering uniform and isothermal loading only. In addition, for the present study, all domains are considered fixed.

[2] In Bottega (1995), 3 regions are considered. Region 2 of the present study corresponds to Region 3 of that study, while Region 1 for the present study corresponds to Region 1 of Bottega (1995). Region 2 of Bottega (1995) is not included presently.

$$u_{\mathrm{p}}^{*}(s) = u_{\mathrm{p}}(x) - \frac{1}{2}h_{\mathrm{p}}w_{\mathrm{p}}', \tag{2b}$$

$$e_i^{*}(x) = e_i(x) + \frac{1}{2}h\kappa_i, \qquad (i = 1, 2) \tag{2c}$$

$$e_{\mathrm{p}}^{*}(x) = e_{\mathrm{p}}(x) - \frac{1}{2}h_{\mathrm{p}}\kappa_{\mathrm{p}}, \tag{2d}$$

where $h \ll 1$ and $h_{\mathrm{p}} \ll 1$ correspond to the normalized thicknesses of the base panel and patch, respectively, and we impose the interface conditions

$$w_1^{*}(x) \equiv w_1(x) = w_{\mathrm{p}}(x), \qquad (x \in S_1), \tag{3a,b}$$

$$\kappa_1^{*}(x) \equiv \kappa_1(x) = \kappa_{\mathrm{p}}(x), \qquad (x \in S_1), \tag{3c,d}$$

$$u_1^{*}(x) = u_{\mathrm{p}}^{*}(x), \qquad (x \in S_1). \tag{3e}$$

At this point, let us also introduce the normalized membrane stiffness C and bending stiffness D of the base panel, and the corresponding normalized membrane and bending stiffnesses, C_{p} and D_{p}, of the patch. The normalization of the stiffnesses of the primitive structures is based on the dimensional bending stiffness, $\bar{D}$, and the dimensional half-span, $\bar{L}$, of the base panel in the undeformed configuration. Hence,

$$C = \frac{12}{h^2}, \tag{4a}$$

$$D = 1, \tag{4b}$$

$$C_{\mathrm{p}} = CE_0h_0, \tag{4c}$$

$$D_{\mathrm{p}} = E_0h_0^3, \tag{4d}$$

$$h_0 = \frac{h_{\mathrm{p}}}{h}, \tag{4e}$$

$$E_0 = \frac{\bar{E}_{\mathrm{p}}}{\bar{E}} \text{ (plane stress)} \tag{4f}$$

or

$$E_0 = \frac{\bar{E}_{\mathrm{p}}/(1-\nu_{\mathrm{p}}^2)}{\bar{E}/(1-\nu^2)} \text{ (plane strain)}, \tag{4f$'$}$$

where $\bar{E}$ and $\bar{E}_{\mathrm{p}}$ correspond to the dimensional elastic moduli of the base panel and patch respectively, and ν and ν_{p} correspond to the associated Poisson's ratios. Similarly, the dimensional in-plane edge load, $\bar{T}$, is related to its non-dimensional counterpart, T_0, as

$$T_0 = \frac{\bar{T}\bar{L}^2}{\bar{D}}. \tag{4g}$$

Likewise, the non-dimensional coefficients of thermal expansion of the base structure and the patch, α^0 and α_p^0 respectively, are the products of the corresponding dimensional coefficients and reference temperature. We correspondingly define, for the present formulation, the augmented coefficients, α and α_p, such that

$$\alpha = \alpha^0 \text{ (plane stress)} \tag{4h}$$

and

$$\alpha_p = \alpha_p^0, \text{ (plane stress)} \tag{4i}$$

or

$$\alpha = (1+\nu)\alpha^0 \text{ (plane strain)} \tag{4h'}$$

and

$$\alpha_p = (1+\nu_p)\alpha_p^0 \text{ (plane strain)} \tag{4i'}$$

We further denote the ratio of coefficients of thermal expansion as α_0, hence

$$\alpha_0 \equiv \frac{\alpha_p}{\alpha}. \tag{4j}$$

Taking the appropriate variations, and invoking the theorem of Stationary Potential Energy, we arrive at the governing differential equations, boundary and matching conditions, and hence arrive at a self-consistent set of equations and conditions. We thus have

$$M_1^{*\prime\prime} - \left(N_1^* w_1^{*\prime}\right)' = 0 \qquad \text{and} \qquad N_1^{*\prime} = 0, \qquad (x \in S_1), \tag{5a,b}$$

$$M_2'' - \left(N_2 w_2'\right)' = 0 \qquad \text{and} \qquad N_2' = 0 \quad (x \in S_2), \tag{6a,b}$$

where

$$N_1^*(x) = C^* e_1^*(x) + B^* \kappa_1^*(x) - n^* \Theta = C^*\left[e_1^*(x) - \alpha^* \Theta\right] + B^*\left[\kappa_1^*(x) - \beta^* \Theta\right] \tag{7a}$$

$$\begin{aligned} M_1^*(x) &= A^* \kappa_1^*(x) + B^* e_1^*(x) - \mu^* \Theta = A^*\left[\kappa_1^*(x) - \beta^* \Theta\right] + B^*\left[e_1^*(x) - \alpha^* \Theta\right] \\ &= D^*\left[\kappa_1^*(x) - \beta^* \Theta\right] + \rho^* N_1^*, \end{aligned} \tag{7b}$$

respectively correspond to the normalized membrane force and normalized bending moment in the patched portion of the composite structure, and

$$N_2(x) = C\left[e_2(x) - \alpha \Theta\right], \tag{8a}$$

$$M_2(x) = D\kappa_2(x) - \frac{1}{2} h N_2, \tag{8b}$$

correspond to the normalized membrane force and normalized bending moment in the base structure outside the patched region.

The stiffnesses and thermal coefficients of the composite structure which occur in Eqs. (7a) and (7b) are found, in terms of the stiffnesses, thermal coefficients, and thicknesses of the substructures, as

$$A^* = D + D_p + \left(\frac{1}{2}h\right)^2 C + \left(\frac{1}{2}h_p\right)^2 C_p, \qquad B^* = \frac{1}{2}h_p C_p - \frac{1}{2}hC, \tag{9a,b}$$

$$C^* = C + C_p, \qquad D^* = A^* - \rho^* B^*, \tag{9c,d}$$

$$\alpha^* = \alpha_1 - \rho^* \beta^*, \qquad \beta^* = \frac{m^*}{D^*}, \tag{9e,f}$$

where

$$\rho^* = \frac{B^*}{C^*}, \qquad \mu^* = \frac{1}{2}h_p C_p \alpha_p - \frac{1}{2}hC\alpha, \tag{9g,h}$$

$$n^* = C_p\alpha_p + C\alpha, \qquad m^* = \mu^* - \rho^* n^*, \qquad \alpha_1 = \frac{n^*}{C^*}. \tag{9i–k}$$

The quantity ρ^* is seen to give the transverse location of the centroid of the composite structure with respect to the reference surface, the parameters α^* and β^* are seen to correspond to the thermal expansion coefficients of the composite structure within the patched region and represent the thermally induced membrane strain at the reference surface and the associated curvature change, respectively, per unit normalized temperature change for a free unloaded structure. The thermal expansion coefficient α_1 is seen to be the corresponding strain per unit temperature at the centroid of the patched segment of an unloaded composite structure.

The associated boundary and matching conditions obtained similarly take the following forms:

$$u_1^*(0) = 0, \qquad w_1^{*\prime}(0) = 0, \qquad \left[M_1^{*\prime} - N_1^* w_1^{*\prime}\right]_{x=0} = 0, \text{ (symmetric deformation)} \tag{10a–c}$$

or

$$\hat{u}_1(0) = \hat{\rho} w_1^{*\prime}(0), \qquad D^*\kappa_1^*(0) = 0, \qquad w_1^*(0) = 0, \text{ (antisymmetric deformation)} \tag{10a′–c′}$$

and

$$u_1^*(L_p) = u_2^*(L_p), \qquad N_1^*(L_p) = N_2(L_p), \tag{11a,b}$$

$$w_1^*(L_p) = w_2(L_p), \qquad w_1^{*\prime}(L_p) = w_2'(L_p), \tag{11c,d}$$

$$M_1^*(L_p) = M_2(L_p), \qquad \left[M_1^{*\prime} - N_1^* w_1^{*\prime}\right]_{x=L_p} = \left[M_2' - N_2 w_2'\right]_{x=L_p}, \tag{11e,f}$$

$$u_2(1) = 0 \quad \text{or} \quad N_2(1) = T_0 \ (T_0 \text{ prescribed}), \tag{12a,a′}$$

and

$$w_2(1) = 0 \quad \text{and} \quad w_2'(1) = 0 \quad \text{or} \quad \kappa_2(1) = 0, \tag{12b,c,c'}$$

where

$$\hat{u}_1(x) = u_1^*(x) + \rho^* w_1^{*\prime}(x) \tag{13a}$$

is the in-plane deflection of the neutral surface of the composite structure in the patched region, and

$$\hat{\rho} \equiv m^* \frac{\Theta}{N_1^*}, \tag{13b}$$

gives the transverse distance from the centroidal plane to the 'effective' neutral plane (i.e., the plane with vanishing moment).

Integration of Eqs. (5b) and (6b), and imposition of the associated matching condition (11b) yields the results

$$N_1^* = N_2 = \text{constant} = -N_0, \tag{14}$$

where $N_0 > 0$ is a (yet to be determined) compressive membrane force.

Finally, integrating the strain–displacement relations and imposing the corresponding boundary and matching conditions for the in-plane displacements results in the *integrability condition* given by

$$u_2(1) - \hat{u}_1(0) = -N_0\left[\frac{L_p^*}{C} + \frac{L_p}{C^*}\right] + \left[L_p^*\alpha + L_p\alpha_1\right]\Theta - \left[\rho^* + \frac{h}{2}\right]w'(L_p) - \sum_{i=1}^{2}\int_{S_i}\frac{1}{2}w_i'^{\,2}\,\mathrm{d}x, \tag{15}$$

where $\hat{u}_1(x)$ is defined by Eq. (13a) and $L_p^* \equiv 1 - L_p$ corresponds to the (half) length of the unpatched segment of the base plate.

The counterparts of Eqs. (5a) and (6a), and the corresponding boundary and matching conditions obtained upon substitution of the result given by Eq. (14), together with the integrability condition (15) transform the problem statement into a mixed formulation in terms of the transverse displacement $w(x)$, the membrane force N_0, and the temperature (change) Θ.

Substituting the expressions for the moments in region 1 and 2, given by Eqs. (7b) and (8b), into the matching condition for the moments over the end of the patch, Eq. (11e), and incorporating Eq. (14), we find that the condition in question takes the form

$$\left[D^*\kappa_1^* - D\kappa_2\right]_{x=L_p} = \mathscr{M}_\lambda, \tag{16}$$

where

$$\mathscr{M}_\lambda \equiv m^*\Theta + \left(\rho^* + \frac{1}{2}h\right)N_0. \tag{17}$$

Upon consideration of the governing differential equations and the remaining boundary and matching conditions augmented by the result in Eq. (14), it may be seen that the parameter $\mathscr{M}_\lambda$, and hence the temperature, appears only at the matching of the moments at the edge of the patch. The parameter $\mathscr{M}_\lambda$ may thus be identified as the 'loading parameter' and is seen to represent the total applied loading acting on the structure. It is thus anticipated that the transverse displacements are proportional to $\mathscr{M}_\lambda$. In this context, $\mathscr{M}_\lambda$ may be interpreted as a moment that is applied at $x = L_p$, due to the mismatch in coefficients of thermal expansion between the patch and the base structure and due to the jump of the neutral surface.

In the next section, the analytical solutions to the non-linear problems of interest are discussed for several support and loading conditions.

3. Analytical solution

In this section, we present analytical solutions for the problems stated in Section 2, for selected boundary and load conditions. As the geometry and material properties of the system are symmetric about the center of its span, we will first be concerned with symmetric solutions. However, we shall also consider the possibility of antisymmetric solutions.

3.1. Symmetric solutions

In this subsection, we present the analytical solution for the non-linear problem presented in Section 2, assuming symmetric deformation. In the case of non-vanishing membrane force, the general solution for the current problem is delineated according to the type of rotational support conditions and is given below.

. *Hinged end conditions*

$$w_1^*(x) = \frac{\mathscr{M}_\lambda}{N_0 \mathscr{H}_{(\mathrm{h})}}\left[\mathscr{H}_{(\mathrm{h})} + \mathscr{A}_1 \cos(k^* x)\right] \qquad (0 \le x \le L_\mathrm{p}), \tag{18a}$$

$$w_2(x) = -\frac{\mathscr{M}_\lambda}{N_0 \mathscr{H}_{(\mathrm{h})}} \mathscr{B}_0 \sin(k(1-x)) \qquad (L_\mathrm{p} \le x \le 1), \tag{18b}$$

where

$$\mathscr{H}_{(\mathrm{h})} = \mathscr{H}_{(\mathrm{h})}(N_0; \mathbf{S}) = \sqrt{\frac{D^*}{D}} \cos\left(k^* L_\mathrm{p}\right)\cos\left(k L_\mathrm{p}^*\right) - \sin\left(k^* L_\mathrm{p}\right)\sin\left(k L_\mathrm{p}^*\right). \tag{19}$$

. *Clamped end conditions*

$$w_1^*(x) = \frac{\mathscr{M}_\lambda}{N_0 \mathscr{H}_{(\mathrm{c})}}\left[\mathscr{H}_{(\mathrm{c})} + \mathscr{A}_2 \cos(k^* x) - \mathscr{B}_0\right] \qquad (0 \le x \le L_\mathrm{p}), \tag{20a}$$

$$w_2(x) = -\frac{\mathscr{M}_\lambda}{N_0 \mathscr{H}_{(\mathrm{c})}} \mathscr{B}_0 [1 - \cos(k(1-x))], \qquad (L_\mathrm{p} \le x \le 1), \tag{20b}$$

where

$$\mathscr{H}_{(\mathrm{c})} = \mathscr{H}_{(\mathrm{c})}(N_0; \mathbf{S}) = \sin\left(k^* L_\mathrm{p}\right)\cos\left(k L_\mathrm{p}^*\right) + \sqrt{\frac{D^*}{D}} \cos\left(k^* L_\mathrm{p}\right)\sin\left(k L_\mathrm{p}^*\right), \tag{21}$$

with

$$\mathscr{A}_1 = -\sqrt{\frac{D^*}{D}}\cos\left(kL_{\mathrm{p}}^*\right), \tag{22a}$$

$$\mathscr{A}_2 = -\sqrt{\frac{D^*}{D}}\sin\left(kL_{\mathrm{p}}^*\right), \tag{22b}$$

$$\mathscr{B}_0 = \sin\left(k^*L_{\mathrm{p}}\right), \tag{22c}$$

$$k^{*2} = \frac{N_0}{D^*} \tag{22d}$$

and

$$k^2 = \frac{N_0}{D}. \tag{22e}$$

In Eqs. (19) and (21), **S** represents the set of stiffnesses of the structure, and we recall that $L_{\mathrm{p}}^* = 1 - L_{\mathrm{p}}$. The general solution given in Eqs. (18–22) is valid for $N_0 > 0$ throughout the structure. For the case of a vanishing membrane force, $N_0 = 0$, the solution is given by

Hinged end conditions

$$w_1^* = \frac{1}{2}\beta^*\Theta\left(x^2 + L_{\mathrm{p}}^2 - 2L_{\mathrm{p}}\right) \qquad (0 \le x \le L_{\mathrm{p}}), \tag{23a}$$

$$w_2 = -\beta^*\Theta L_{\mathrm{p}}(1-x) \qquad (L_{\mathrm{p}} \le x \le 1), \tag{23b}$$

Clamped end conditions

$$w_1^* = -\frac{1}{2}\beta^*\Theta\left[(B_0 - 1)x^2 + L_{\mathrm{p}}A_0\right], \quad (0 \le x \le L_{\mathrm{p}}), \tag{24a}$$

$$w_2 = -\frac{1}{2}\beta^*\Theta\frac{D^*}{D}(1-x)^2 B_0, \quad (L_{\mathrm{p}} \le x \le 1), \tag{24b}$$

where

$$A_0 = \frac{L_{\mathrm{p}}^* D^*}{L_{\mathrm{p}}^* D^* + L_{\mathrm{p}} D} \tag{24c}$$

and

$$B_0 = \frac{L_{\mathrm{p}} D}{L_{\mathrm{p}}^* D^* + L_{\mathrm{p}} D}. \tag{24d}$$

If, for any of the cases considered above (Eqs. (18–24)), the edges of the base panel are free to translate in the plane, the corresponding in-plane edge deflection may be found upon substitution of the appropriate solution into the integrability condition (15). For the case where the edges are fixed with regard to in-plane motion, Eq. (15) will give the non-trivial relationship between the membrane force

and the temperature for each of the solutions presented above. For the latter case, the integrability condition may be solved numerically for the membrane force N_0, for a given temperature Θ.

Eqs. (18a,b), (20a,b) possess three important quantities, $\mathscr{M}_\lambda$, $\mathscr{H}_{(h)}(N_0; \mathbf{S})$ and $\mathscr{H}_{(c)}(N_0; \mathbf{S})$, where the former is defined in Eq. (17) and the latter two in Eqs. (19) and (21), respectively. The significance of these quantities is discussed below. For ease of presentation, we drop the subscripts associated with the particular type of rotational edge condition and refer to a generic $\mathscr{H}(N_0; \mathbf{S})$ in the following discussion. It may be seen from Eqs. (18a), (18b), (20a) and (20b) that if the pertinent function $\mathscr{H}(N_0; \mathbf{S})$ approaches zero, the deflections become large, and that when $\mathscr{H}(N_0; \mathbf{S})$ vanishes, the deformation becomes singular (i.e., is undefined). The membrane force associated with the singular case will be seen to be associated with a bifurcation in the loading path for the case of controlled edge force loading (free in-plane edge conditions), and with the onset of 'sling-shot buckling' for the case of temperature controlled loading with fixed in-plane edge conditions. The equation

$$\mathscr{H}(N_0, \mathbf{S}) = 0 \tag{25}$$

may, therefore, be interpreted as the associated 'characteristic equation'. A compressive membrane force satisfying the characteristic equation will be referred to as a 'critical membrane force', and will therefore be denoted as N_{cr}. There is evidently more than one such membrane force for a given structure. It may be noted that if we let the length of the patch vanish ($L_p \to 0$) in Eqs. (19) and (21), Eq. (25) assumes the forms of the characteristic equations associated with 'Euler buckling'. Furthermore, it may be seen from Eqs. (19) and (21) that N_{cr} is independent of the temperature and the coefficients of thermal expansion.

As was anticipated in Section 2, the solutions of Eqs. (18–24) are seen to be proportional to the parameter $\mathscr{M}_\lambda$, where $\mathscr{M}_\lambda$, as defined by Eq. (17), is proportional to N_0 and Θ. It is further seen from these solutions that vanishing load parameter, $\mathscr{M}_\lambda = 0$, is associated with vanishing of the transverse displacement over the entire span of the structure. Hence, the vanishing of the loading parameter is associated with flat configurations of the deforming structure. However, it may be seen from Eq. (17) that $\mathscr{M}_\lambda$ vanishes for an appropriate ratio of N_0 and Θ provided $m^*\Theta < 0$ for a given structure. Hence, flat configurations other than those corresponding to the trivial case ($N_0 = \Theta = 0$) are possible for structures for which $m^*\Theta$ is negative definite. Therefore, if a structure is supported in such a manner that the edges of the base plate are free for in-plane motion, a loading program may be constructed in such a way that the structure remains flat throughout the loading sequence. Alternatively, such a structure may be subjected to temperature controlled loading with N_0 fixed or N_0 controlled loading with Θ fixed, with a flat configuration eventually being realized when the critical ratio of Θ and N_0 is achieved. For the situations where the edges of the base plate are fixed with regard to in-plane motion, the membrane force and temperature cannot be prescribed independently. Rather, the membrane force, N_0, is a nonlinear function of the temperature, Θ, obtained by substitution of the solution for the transverse displacement, Eqs. (18a) and (18b) or Eqs. (20a) and (20b), into the integrability condition (15) with $u_2(1) \equiv 0$. As the condition for uniformly flat equilibrium configurations, $\mathscr{M}_\lambda = 0$, results in a linear relation between N_0 and Θ, it is evident that this relation can intercept the transcendental equation resulting from the integrability condition at a discrete number of points. Hence, when the support conditions prohibit in-plane translation, a continuous loading path accompanied by uniformly vanishing transverse deflection is not possible.

For the special case when $\mathscr{M}_\lambda$ indeed vanishes, we may solve for the corresponding ratio of temperature and membrane force using Eq. (17). For the particular case where $N_0 = N_{cr}$, the corresponding temperature $\Theta = \Theta_{cr}$, is given by

$$\Theta_{\mathrm{cr}} = -\frac{\rho^* + \frac{1}{2}h}{m^*} N_{\mathrm{cr}}. \tag{26}$$

It will be seen in Section 5 that this temperature is closely associated with the characterization of the structural response of the composite system and hence is designated as the 'critical temperature'.

Finally, let us consider the case when both the loading parameter, $\mathscr{M}_\lambda$, and the characteristic function, $\mathscr{H}(N_0; \mathbf{S})$, vanish simultaneously. The solution for the transverse deflection for this case is

Hinged end conditions

$$w_1^*(x) = A_0(\mathscr{A}_1/\mathscr{B}_0)\cos(k^* x), \qquad (0 \le x \le L_{\mathrm{p}}), \tag{27a}$$

$$w_2(x) = -A_0 \sin(k(1-x)), \qquad (L_{\mathrm{p}} \le x \le 1), \tag{27b}$$

Clamped end conditions

$$w_1^*(x) = A_0\big[-1 + (\mathscr{A}_2/\mathscr{B}_0)\cos(k^* x)\big], \qquad (0 \le x \le L_{\mathrm{p}}), \tag{28a}$$

$$w_2(x) = -A_0[1 - \cos(k(1-x))] \qquad (L_{\mathrm{p}} \le x \le 1), \tag{28b}$$

where A_0 is an arbitrary constant and $\mathscr{A}_1$, $\mathscr{A}_2$ and $\mathscr{B}_0$ are given by Eqs. (22a), (22b) and (22c) respectively. Thus, the deflection is determined to its shape but not to its magnitude for the case where the edges of the structure are free to translate in-plane. If the in-plane deflection of the edges is prescribed, the integrability condition (15) provides one more condition to be satisfied. By substituting Eqs. (27a) and (27b) or Eqs. (28a) and (28b) into Eq. (15), a polynomial of the second degree with respect to A_0 is obtained, and the unknown constant A_0 may be determined, for a given temperature Θ. Hence, for the case of $\mathscr{M}_\lambda = 0$, $\mathscr{H}(N_0; \mathbf{S}) = 0$ and prescribed in-plane edge deflections, the constant A_0 may assume two different values. It will be seen in Section 5 that this case corresponds to the onset of 'sling-shot buckling'.

We next examine the existence of antisymmetric solutions for the problem of interest.

3.2. Existence of antisymmetric solutions

The general solutions to the governing differential equations (Eqs. (5a) and (6a)), may be expressed as the sum of two parts: a symmetric part, w_{S} and an antisymmetric part w_{AS}. Thus,

$$w(x) = w_{\mathrm{S}}(x) + w_{\mathrm{AS}}(x). \tag{29}$$

In Eq. (29), the denotation of the particular region of the structure has been omitted for simplicity. While the matching conditions for the transverse displacement Eq. (11c), rotation Eq. (11d) and transverse shear Eq. (11f) are satisfied passively by the form (29), the condition for moment Eq. (11e) warrants a detailed discussion.

We recall that the curvature for a plate is given by $\kappa = w''$, hence if $w(x)$ is a symmetric (even) function, then $\kappa(x)$ is even, and if $w(x)$ is an antisymmetric (odd) function, then $\kappa(x)$ is also odd[3].

[3] It may be easily shown that, for a function with sufficient number of non-vanishing derivatives, the derivative of an odd function is even, and vice versa, hence the second derivative of an odd function is odd and the second derivative of an even function is even.

Hence, when separating the solution into symmetric and antisymmetric parts, Eq. (16) may be written as

$$D^*\kappa^*_{1_S}(L_p) - D\kappa_{2_S}(L_p) = \mathscr{M}_{\lambda_S} \tag{30a}$$

and

$$D^*\kappa^*_{1_{AS}}(L_p) - D\kappa_{2_{AS}}(L_p) = \mathscr{M}_{\lambda_{AS}}, \tag{30b}$$

where $\mathscr{M}_{\lambda_S}$ and $\mathscr{M}_{\lambda_{AS}}$ denote the loading parameters for the symmetric problem and for the antisymmetric problem, respectively. Since the geometry and stiffnesses of the system are symmetric, and since N_0 and Θ are both uniform, the loading parameter, $\mathscr{M}_\lambda = \mathscr{M}_{\lambda_S} + \mathscr{M}_{\lambda_{AS}}$, may be seen to be symmetric as well. Hence, $\mathscr{M}_\lambda \equiv \mathscr{M}_{\lambda_S}$ and $\mathscr{M}_{\lambda_{AS}}$ vanishes. The matching condition for the moment at $x = L_p$ for the antisymmetric case, thus becomes

$$D^*\kappa^*_{1_{AS}}(L_p) - D\kappa_{2_{AS}}(L_p) = 0. \tag{30b′}$$

From Eq. (30b′), it follows that only two types of antisymmetric solutions are possible for the current problem: the trivial solution, where there is no transverse displacement ($w \equiv 0$), and non-trivial solutions for which $N_0 = N_{cr_{AS}}$ (where $N_{cr_{AS}}$ is defined in a manner similar to that defined for the symmetric case). Paralleling the discussion regarding vanishing transverse displacements for the symmetric case, it follows that $w(x) = 0$, $\forall x \in [0, 1]$, for the antisymmetric case can exist for non-vanishing temperature and/or membrane force only when the edges of the base plate are free to allow in-plane motion. Thus, it may be seen that a loading program may be prescribed such that the ratio of compressive force to temperature satisfies Eq. (30b′). With this ratio of N_0 to Θ, the structure will remain flat as the load progresses, until the critical compressive force $N_{cr_{AS}}$ is reached. At this point, it is anticipated that the structure will buckle in an antisymmetric mode. As discussed in the preceding section, for the case where the edges are fixed so as to prohibit motion in the plane, there exist only discrete combinations of N_0 and Θ, given by the integrability condition. Thus, the above mentioned loading scenario is not possible if the edges are 'fixed'. However, it may be noted from Eq. (29) that an antisymmetric solution may be superposed on a symmetric solution, which implies that it is possible for a symmetrically deformed structure to buckle in an antisymmetric manner, once the critical load $N_{cr_{AS}}$ is reached.

The critical load, $N_{cr_{AS}}$, may be found from the 'characteristic equation' for antisymmetric solutions,

$$\mathscr{H}_{AS}(N_0; \mathbf{S}) = 0, \tag{31}$$

where $\mathscr{H}_{AS}(N_0; \mathbf{S})$ is dependent on the support conditions as follows:

Hinged end conditions

$$\mathscr{H}_{AS} = \mathscr{H}_{(h)}(N_0; \mathbf{S}) = \sin\left(k^* L_p\right)\cos\left(kL^*_p\right) + \sqrt{\frac{D}{D^*}}\cos\left(k^* L_p\right)\sin\left(kL^*_p\right), \tag{32}$$

Clamped end conditions

$$\begin{aligned}\mathscr{H}_{AS} &= \mathscr{H}_{(c)}(N_0; \mathbf{S}) \\ &= \left[\sin\left(kL^*_p\right) - k\cos\left(kL^*_p\right)\right]\sqrt{\frac{D}{D^*}}\cos\left(k^* L_p\right) + \left[k\sin\left(kL^*_p\right) + \cos\left(kL^*_p\right)\right]\sin\left(k^* L_p\right).\end{aligned} \tag{33}$$

Since the non-linearity of the problem may result in multiple solutions (i.e., multiple equilibrium

configurations for a given value of the loading parameter) stability of the equilibrium configurations must be addressed. This is done in the next section.

4. Stability criterion

It was seen in prior sections that multiple equilibrium configurations of the structure are possible for a given value of the loading parameter. It is therefore of interest to determine which of the configurations are stable and which are unstable. In this regard, stability will be assessed by examination of the second variation of the potential energy of the system, Π. A particular equilibrium configuration will be considered stable if $\delta^2\Pi$ (where δ corresponds to the variational operator) is positive definite for that state in the context of perturbations away from it (see, for example, Simitses, 1986). Thus, if

$$\delta^2\Pi > 0, \tag{34}$$

the configuration will be said to be stable. If not, it will be considered unstable. For the system under consideration, the second variation takes the form

$$\begin{aligned}\delta^2\Pi = &\int_{S_1} \frac{1}{2}D^*\left(\delta w_1^{*\prime\prime}\right)^2 \mathrm{d}x + \int_{S_1} \frac{1}{2}\left[- N_0\left(\delta w_1^{*\prime}\right)^2 + \frac{1}{C^*}(\delta N_0)^2 \right]\mathrm{d}x + \int_{S_2} \frac{1}{2}D(\delta w_2^{*\prime\prime})^2 \,\mathrm{d}x \\ &+ \int_{S_2} \frac{1}{2}\left[- N_0\left(\delta w_2'\right)^2 + \frac{1}{C}(\delta N_0)^2 \right]\mathrm{d}x,\end{aligned} \tag{35}$$

where the temperature is assumed to be prescribed.

We will perturb the system away from its equilibrium configuration by applying a small moment about an axis through the reference surface at the edge of the patch, $x = L_{\mathrm{p}}$. (One might imagine a screwdriver applied to an embedded and perfectly bonded screw at the point in question). If it can be concluded that the system returns to the equilibrium state in question upon release of the moment, the configuration associated with this state will be considered stable. If it moves away from this state it will be considered unstable. Mathematically, such a moment manifests itself as a variation of the loading parameter, $\mathscr{M}_\lambda$ (i.e., as $\delta\mathscr{M}_\lambda$) in the amplitude of the solution for the transverse displacement given by Eqs. (18a), (18b), (20a) and (20b). The second variation of the potential energy is evaluated by substituting the corresponding variation of the transverse deflection (the 'perturbed' response) into Eq. (35). Stability of a given configuration may then be assessed by evaluating the resulting expression at a given state of equilibrium, and applying the criterion expressed by Eq. (34). This may be done for any range of points on any equilibrium path.

After performing the substitution described above, Eq. (35) takes the form

$$\delta^2\Pi = \frac{\mathscr{F}}{N_0}(\delta\mathscr{M}_\lambda)^2 + \zeta(\delta N)^2, \tag{36}$$

where

$$\mathscr{F} = \frac{1}{4}\left(f_{\mathscr{A}}^{\,2}k^* \sin 2k^*L_{\mathrm{p}} + f_{\mathscr{B}}^{\,2}k \sin 2kL_{\mathrm{p}}^*\right) \tag{37}$$

$$\zeta = \frac{1}{2}\left(\frac{L_{\mathrm{p}}}{C^*} + \frac{L_{\mathrm{p}}^*}{C}\right), \tag{38}$$

with

$$f_{\mathscr{A}} = \frac{\mathscr{A}_1}{\mathscr{H}_{(h)}}, \qquad f_{\mathscr{B}} = \frac{\mathscr{B}_0}{\mathscr{H}_{(h)}} \quad \text{(hinged end conditions)}, \tag{39a,b}$$

or

$$f_{\mathscr{A}} = \frac{\mathscr{A}_2}{\mathscr{H}_{(c)}}, \qquad f_{\mathscr{B}} = \frac{\mathscr{B}_0}{\mathscr{H}_{(c)}} \quad \text{(clamped end conditions)}, \tag{40a}$$

$\mathscr{A}_1$, $\mathscr{A}_2$ and $\mathscr{B}_0$ defined by Eqs. (22a), (22b) and (22c), and $\mathscr{H}_{(h)}$ and $\mathscr{H}_{(c)}$ defined by Eqs. (19) and (21) respectively. To establish if Eq. (36) is positive definite, we write the expression in canonical form and use Sylvester's criterion (see, for example, Gelfand and Fomin, 1963). In doing so, we thus require that

$$\begin{vmatrix} \dfrac{\mathscr{F}}{N_0} & 0 \\ 0 & \zeta \end{vmatrix} > 0 \quad \text{and} \quad \frac{\mathscr{F}}{N_0} > 0 \tag{41}$$

for a stable equilibrium configuration. Since it may be readily seen that $\zeta > 0$ and since the solution corresponds to $N_0 > 0$, the requirement for stability is simply that $\mathscr{F}$ must be positive definite, i.e.,

an equilibrium configuration is stable if $\mathscr{F} > 0$, (42)

where $\mathscr{F}$ is given by Eq. (37).

With the analytical solution and stability criterion established, we next present results of numerical simulations which elucidate the structural behavior of the patched plate.

5. Results and discussion

In this section, results are presented for patched plates subjected to a uniform applied temperature field, $\Theta > 0$, under various loading scenarios and support conditions. With regard to the latter, we consider plates where the edges are either hinged or clamped with regard to rotations and are either free or fixed with regard to in-plane translation. In each case the analytical solutions based on the non-linear formulation presented earlier are employed. For the case where the edges are free to allow in-plane motion, we consider an in-plane compressive force applied at the edge of the structure and examine the behavior of the composite structure for a range of loading situations. For the case where the edges are fixed so as to prohibit in-plane motion we examine the temperature controlled behavior of the composite structure.

Detailed results for representative patched plates, which elucidate the characteristic behavior of structures of the class of interest, are presented and discussed in Section 5.1. These results are extended to a broad range of structures in Section 5.2 by examining the behavior of the characteristic parameters N_{cr} and Θ_{cr} for a wide range of structural properties. To fully investigate the behavior of the patched plate under loading, we consider various normalized lengths of the patch, L_p, as well as various ratios of the coefficients of the thermal expansion, α_0.

5.1. Loading scenarios

We next present selected results for various load cases for a range of structures. For brevity, we limit

our discussion to the representative cases where the ratio of thermal expansion coefficients is $\alpha_0 = 1/2$, 1 and 2. We likewise restrict the current discussion to the representative case of patches of length $L_p = 0.8$, modulus ratio $E_0 = 1$ and thicknesses $h_p = h = 0.05$. Similar results are found when the structural and thermal parameters are varied, but are omitted for brevity.

5.1.1. Edges free to translate in-plane

In this subsection, we consider the case where the edges are free to allow in-plane deflections. For this case, we will be concerned with three types of loading scenarios:

(i) a plate subjected to a constant temperature field and a controlled in-plane edge force,
(ii) a plate subjected to a controlled in-plane edge force and a controlled uniform (positive) temperature such that the loading parameter maintains a constant value, and
(iii) a plate subjected to a constant in-plane edge force and a controlled uniform (positive) temperature field.

5.1.1.1. Edge force controlled loading in a fixed temperature field. We consider the case where the plate is loaded with a compressive edge force under a constant positive temperature field. The normalized compressive membrane force, N_0, is displayed as a function of the in-plane edge-deflection, $u_L \equiv u_2(1)$, for hinged and clamped edge conditions in Fig. 2 and 3, respectively, for a range of temperatures. (We recall that 'temperature' in this context corresponds to the normalized temperature change above a reference, as defined in Section 2). In Fig. 2(a) and Fig. 3(a), the load paths are displayed for $\alpha_0 = 1/2$, in Fig. 2(b) and Fig. 3(b) for $\alpha_0 = 1$, and in Fig. 2(c) and Fig. 3(c) for $\alpha_0 = 2$. For each case, it may be seen upon following an isotherm, that for vanishing membrane force, there will be an initial in-plane deformation which is positive (extensive), $u_L > 0$. This corresponds to the deformation due to thermal effects alone. When a compressive in-plane force is applied, u_L is seen to decrease, eventually achieving negative deflection as the magnitude of the force is increased. When a certain level of the membrane force is approached, the deflection is seen to increase in a relatively rapid fashion with increasing force, with the force evidently approaching a limiting value. The 'limiting force' may be seen to be independent of Θ and α_0 and is found to have the numerical values of $N_0 = 17.8$ for hinged support conditions and $N_0 = 36.3$ for clamped support conditions. The high rate of deformation may be interpreted as buckling of the structure, and the 'limiting force' as a buckling load. We shall refer to this type of behavior as 'asymptotic buckling'. The 'limiting force', observed in Figs. 2 and 3, is seen to coincide with the critical membrane force discussed in Section 3. It may be seen in Fig. 2 and 3 that a second 'limiting force' may be found at $N_{cr} = 81.3$ and 194.6, respectively, which corresponds to the second critical membrane force. However, it will be seen next that under edge force controlled loading, membrane forces higher than the lowest critical force may not be reached in the case of kinematically free boundaries[4]. The critical membrane force as defined by Eq. (25) is thus seen to correspond to a buckling load of the structure under force controlled edge loading as suggested in Section 3.

Consider next the corresponding transverse centerspan deflections. As indicated for the associated in-plane deflections, the general qualitative behavior is independent of the manner in which the edges are supported with regard to rotations. Hence, we limit our discussion to the case of clamped edges, for brevity. In Fig. 4(a,b), the compressive membrane force, N_0, is displayed as a function of the centerspan deflection $w_0 \equiv w_1^*(0)$ for a range of temperatures, for the ratio of thermal expansion coefficients $\alpha_0 = 1/2$ and 2, respectively. We recall that the critical membrane force for this case is $N_{cr} = 36.3$.

[4] Unless the system is artificially constrained until the first N_{cr} is surpassed.

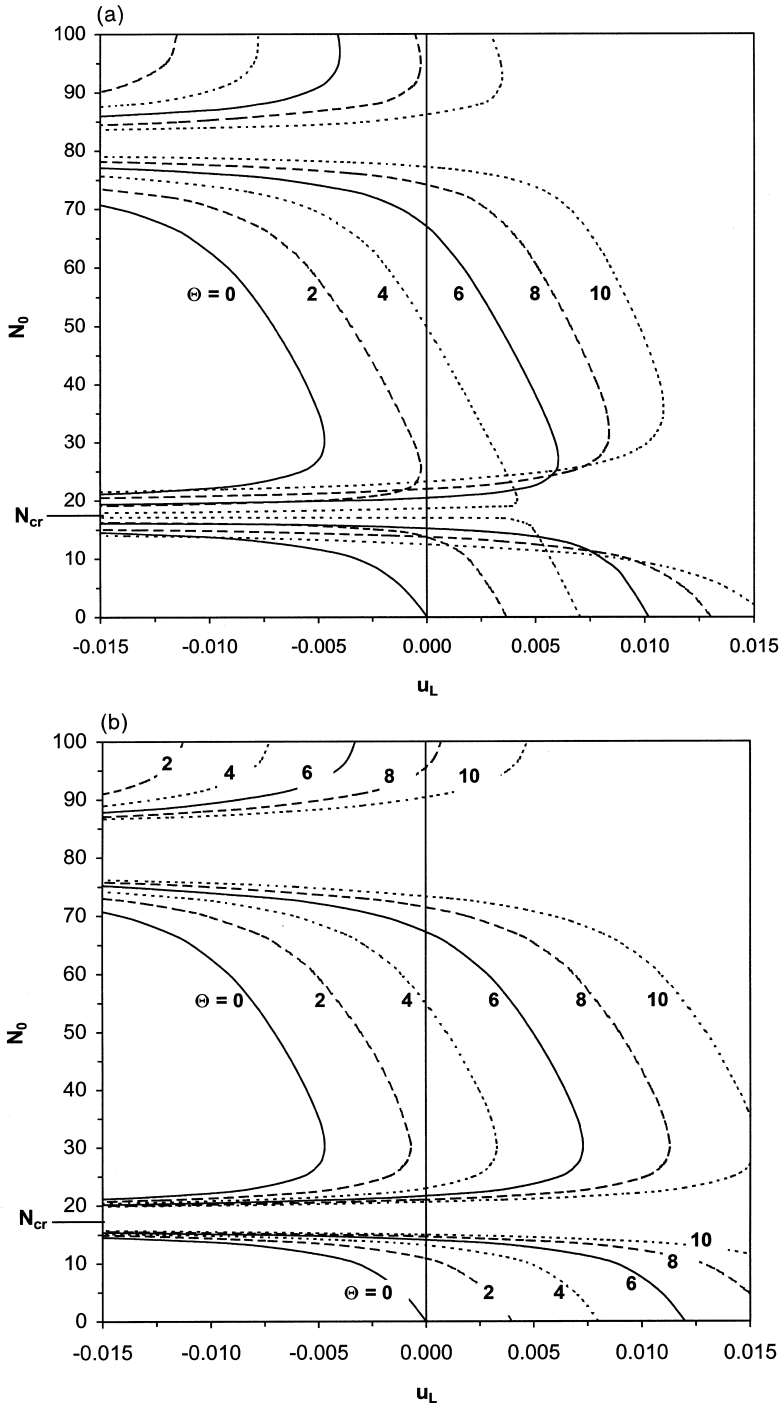

Fig. 2. Normalized compressive membrane force, N_0, vs. normalized in-plane edge displacement, u_L, for various values of the normalized temperatures, Θ; (a) $\alpha_0 = 1/2$, (b) $\alpha_0 = 1$, (c) $\alpha_0 = 2$. (*Hinged supports*, $L_p = 0.8$, $E_0 = 1$).

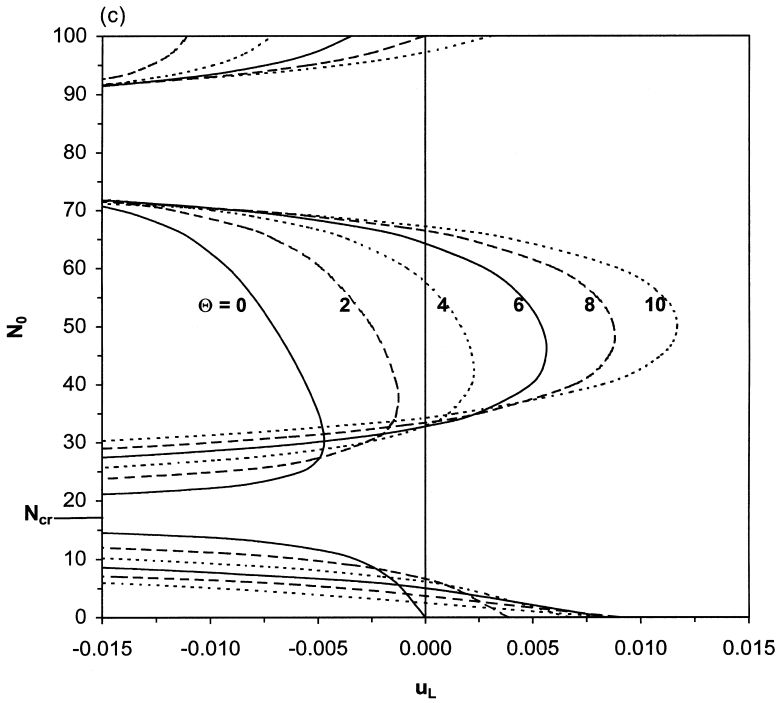

Fig. 2 (*continued*)

Consider now the case of $\alpha_0 = 1/2$ [Fig. 4(a)]. For a vanishing membrane force, it may be seen that the centerspan has an initial positive deflection (downwards), corresponding to the temperature effects alone. When the edges of the plate are subsequently loaded with a compressive in-plane force it may be seen that as the membrane force increases the centerspan deflection changes first moderately, but as the value of the edge load approaches N_{cr} the deflection becomes large and the structure in effect buckles ('asymptotic buckling'), as may be anticipated from the discussion concerning the in-plane deflection. However, the sense of the centerspan deflection, as N_{cr} is approached, is seen to depend on the magnitude of the temperature. It may be seen that if the temperature field is less than a certain value of the temperature, in this case $\Theta < 7.57$, the centerspan will deflect upward (negative values) and for $\Theta > 7.57$, the centerspan will deflect downwards. When $\Theta \approx 7.57$, the centerspan deflection will change very little until the critical membrane force is reached. At this point, the deflection becomes undetermined, within the context of the present mathematical model, and bifurcation buckling occurs. We may recall that in Section 3, a 'critical temperature', Θ_{cr}, was introduced in Eq. (26). For the structure under consideration, and with $\alpha_0 = 1/2$, it may be seen that the critical temperature is given by $\Theta_{cr} = 7.57$. Thus, it may be concluded[5] that the critical temperature divides the structural behavior between upward and downward deflection changes. It may further be noted that the membrane force may never exceed the critical membrane force in the loading scenario described.

It was shown in Section 3 that for structures where $\alpha_0 \geq 1$ (i.e. $m^* \geq 0$)[6], a (positive) critical

[5] Similar results are found for a variety of combinations of relative patch lengths and ratios of coefficients of thermal expansion. Likewise, similar behavior is observed for structures with hinged edges. Such results are omitted for brevity.

[6] It follows from Eqs. 9a–k, and (4j) that if $\alpha_0 = 1$ then $m^* = 0$, if $\alpha_0 < 1$, then $m^* < 0$ and if $\alpha_0 > 1$, then $m^* > 0$.

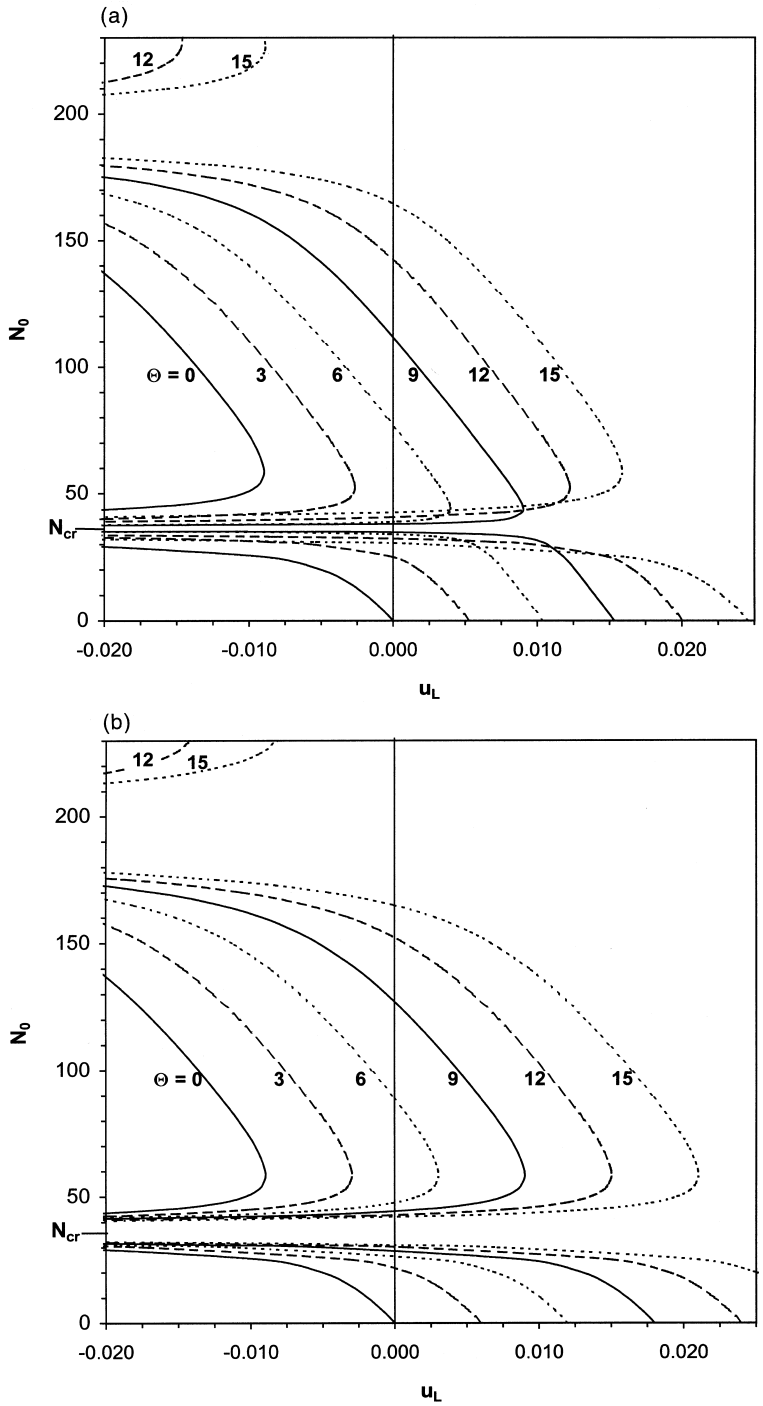

Fig. 3. Normalized compressive membrane force, N_0, vs. normalized in-plane edge displacement, u_L, for various values of the normalized temperatures, Θ; (a) $\alpha_0 = 1/2$, (b) $\alpha_0 = 1$, (c) $\alpha_0 = 2$. (*Clamped supports*, $L_p = 0.8$, $E_0 = 1$).

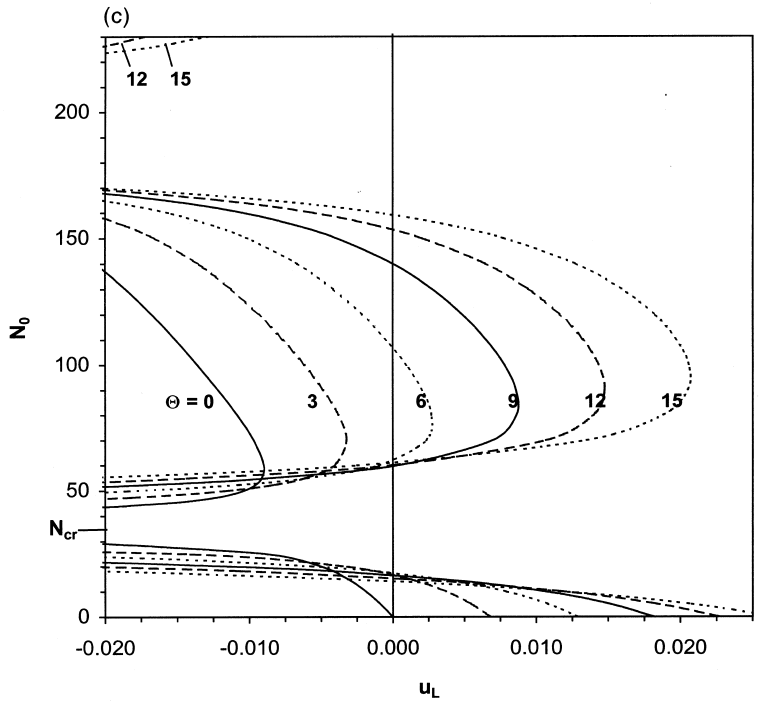

Fig. 3 (*continued*)

temperature does not exist. We recall that for such cases, the load parameter will only vanish for the trivial case ($N_0=0$, $\Theta=0$). In the limiting case, where $\alpha_0=1$ ($m^*=0$), it may be seen from Eq. (17) that the load parameter depends on the membrane force alone. Thus, for this case, the transverse deflection of the plate is independent of the temperature and it may be easily verified that the plate deflects upwards as the in-plane edge load is applied. Upon consideration of Fig. 4(b), which displays the membrane force as a function of the transverse centerspan deflection for a range of temperatures for $\alpha_0=2$, it may be seen that the structure deflects upwards for all load combinations.

The fact that the transverse deflection is negative for $\Theta < \Theta_{cr}$ (for large enough N_0) and positive otherwise, in the case of $\alpha_0 < 1$, may be explained in the following manner. Consider a patch that has a coefficient of thermal expansion less than that of the base structure (i.e., $\alpha_0 < 1$). If the structure is subjected to a temperature field alone (vanishing membrane force), the mismatch in thermal expansion coefficients leads to downward deflections of the plate (i.e., w positive). This is supported by Fig. 4(a) ($\alpha_0=1/2$), when $N_0=0$. However, when the plate is loaded with only a compressive membrane force (vanishing temperature), the plate will tend to deflect upward (w negative). This again is supported by Fig. 4(a), for the isotherm $\Theta=0$. When the plate is loaded with a combination of membrane force and temperature, the tendency for the temperature to induce positive deflection 'competes' with the tendency for the membrane force to induce negative deflection. When $\Theta < \Theta_{cr}$, the membrane force is seen to prevail, and hence it governs the direction of the transverse deflection. For $\Theta > \Theta_{cr}$, the opposite is true. In the case of a vanishing load parameter ($\mathcal{M}_\lambda=0$), the deflections associated with temperature and those associated with the membrane force cancel one another, producing vanishing transverse displacement. For the structures that do not possess a positive critical temperature, ($\alpha_0 \geq 1$), the deflections associated with temperature and with membrane force reinforce each other and hence induce deflections in the same direction.

5.1.1.2. Edge force controlled loading with fixed loading parameters. Let us consider the case where the temperature, Θ, and membrane force, N_0, are controlled in such a manner that the loading parameters, $\mathscr{M}_\lambda$, will remain constant. In particular, if N_0 is increased monotonically, the value of Θ, or more generally the value of $m^*\Theta$, required to maintain $\mathscr{M}_\lambda$ at a constant value may be determined by Eq. (17). In Fig. 5, the membrane force, N_0, is displayed as a function of the centerspan deflection, w_0, for various values of the load parameter, $\mathscr{M}_\lambda$. The path corresponding to the case of $m^*\Theta = 0$ is also displayed. Depending on the value of m^*, Fig. 5 may be interpreted as described in the following.

If the composite structure under consideration corresponds to one where $m^* < 0$ ($\alpha_0 < 1$) then all load

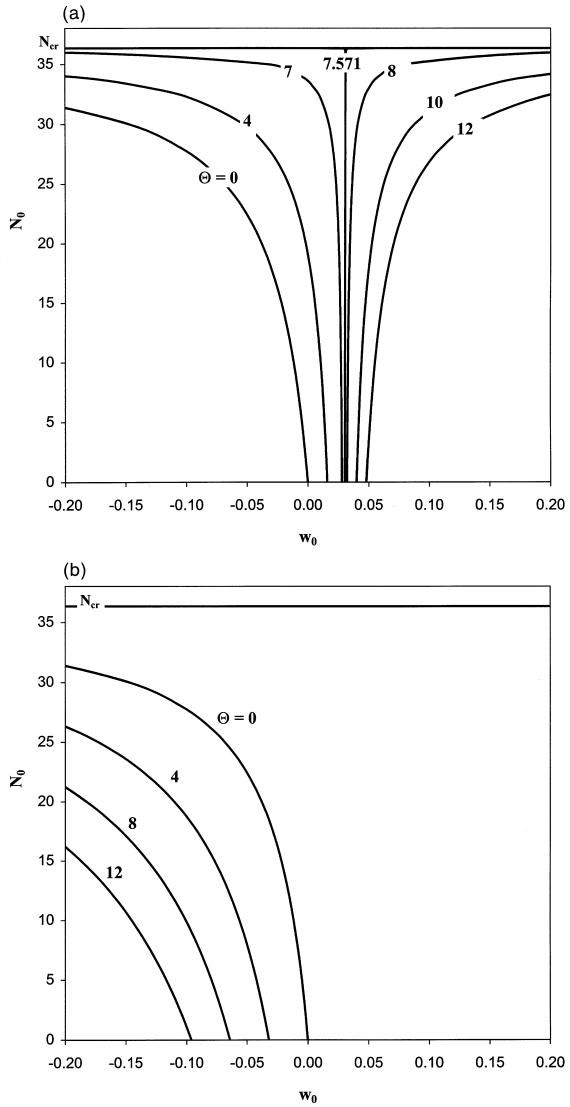

Fig. 4. Normalized compressive membrane force, N_0, vs. normalized transverse centerspan displacement, w_0, for various values of the normalized temperatures, Θ; (a) $\alpha_0 = 1/2$, (b) $\alpha_0 = 2$. (*Clamped-Free supports*, $L_p = 0.8$, $E_0 = 1$).

paths, or portions of load paths, that are located above and to the right of $m^*\Theta = 0$ correspond to positive temperatures. The load paths below and to the left of $m^*\Theta = 0$ correspond to negative temperatures, and are thus not considered in this study. Obviously, in this case, the curve $m^*\Theta = 0$ must correspond to $\Theta = 0$. If, instead, the composite structure corresponds to one where $m^* > 0$ ($\alpha_0 > 1$) the opposite is true; paths corresponding to positive temperatures are situated below and to the left of the curve $m^*\Theta = 0$ (i.e., $\Theta = 0$). For the case when the patch has the same coefficient of thermal expansion as the base structure ($m^* = 0$ and, equivalently, $\alpha_0 = 1$) the curve $m^*\Theta = 0$ corresponds to $m^* = 0$. Thus, for this case, the transverse displacement as a function of increasing membrane force is given by the curve $m^*\Theta = 0$ and it may be seen that a constant value of the loading parameter cannot yield permissible solutions for this case.

With the above described interpretations of Fig. 5 in mind, we may consider the general behavior as characterized by the centerspan deflections, w_0, for a constant loading parameter, $\mathscr{M}_\lambda$, and a monotonically increasing membrane force, N_0. From Fig. 5, it may be seen that the case of vanishing loading parameter corresponds to a uniformly vanishing deflection, as was anticipated in Section 3. For this case, the critical membrane force, N_{cr}, corresponds to a bifurcation point. Thus once the critical membrane force is achieved, bifurcation buckling occurs. For non-vanishing loading parameters, it may be seen that $\mathscr{M}_\lambda < 0$ corresponds to upward deflections of the structure, while $\mathscr{M}_\lambda > 0$ corresponds to downward deflections. For either case, the deflections become large as the critical membrane force is approached so that the structure, in effect, buckles ('asymptotic buckling') and N_{cr} is never exceeded. Furthermore, it may be noted that the magnitude of the centerspan deflection is symmetric with respect to the loading parameter [i.e., $|w_0(-\mathscr{M}_\lambda)| = |w_0(\mathscr{M}_\lambda)|$]. Comparing the present results to the classical results for (unpatched) beam-plates, it may be seen that the magnitude of $\mathscr{M}_\lambda$ describes how far the structure is from being 'perfect', with $\mathscr{M}_\lambda = 0$ corresponding to a 'perfect' structure.

5.1.1.3. Temperature controlled loading. We next consider the case where the plate is subjected to a constant in-plane edge force and loaded with a uniformly changing temperature field. Fig. 6(a–c) display the temperature, Θ, as a function of the centerspan deflection, w_0, for a range of values of the normalized

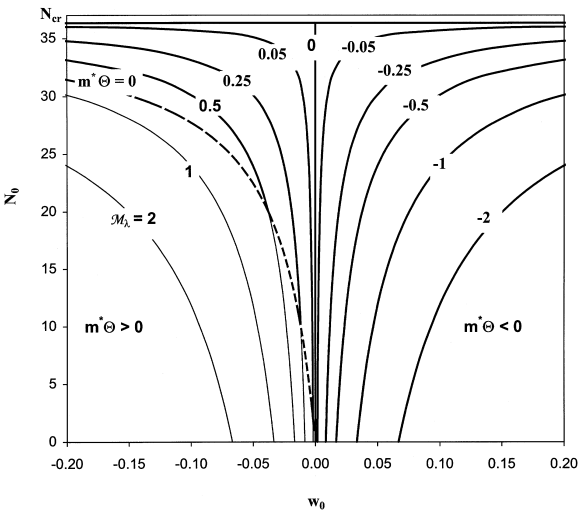

Fig. 5. Normalized compressive membrane force, N_0, vs. normalized transverse centerspan displacement, w_0, for various values of the loading parameter, $\mathscr{M}_\lambda$. (*Clamped-Free supports*, $L_p = 0.8$, $E_0 = 1$).

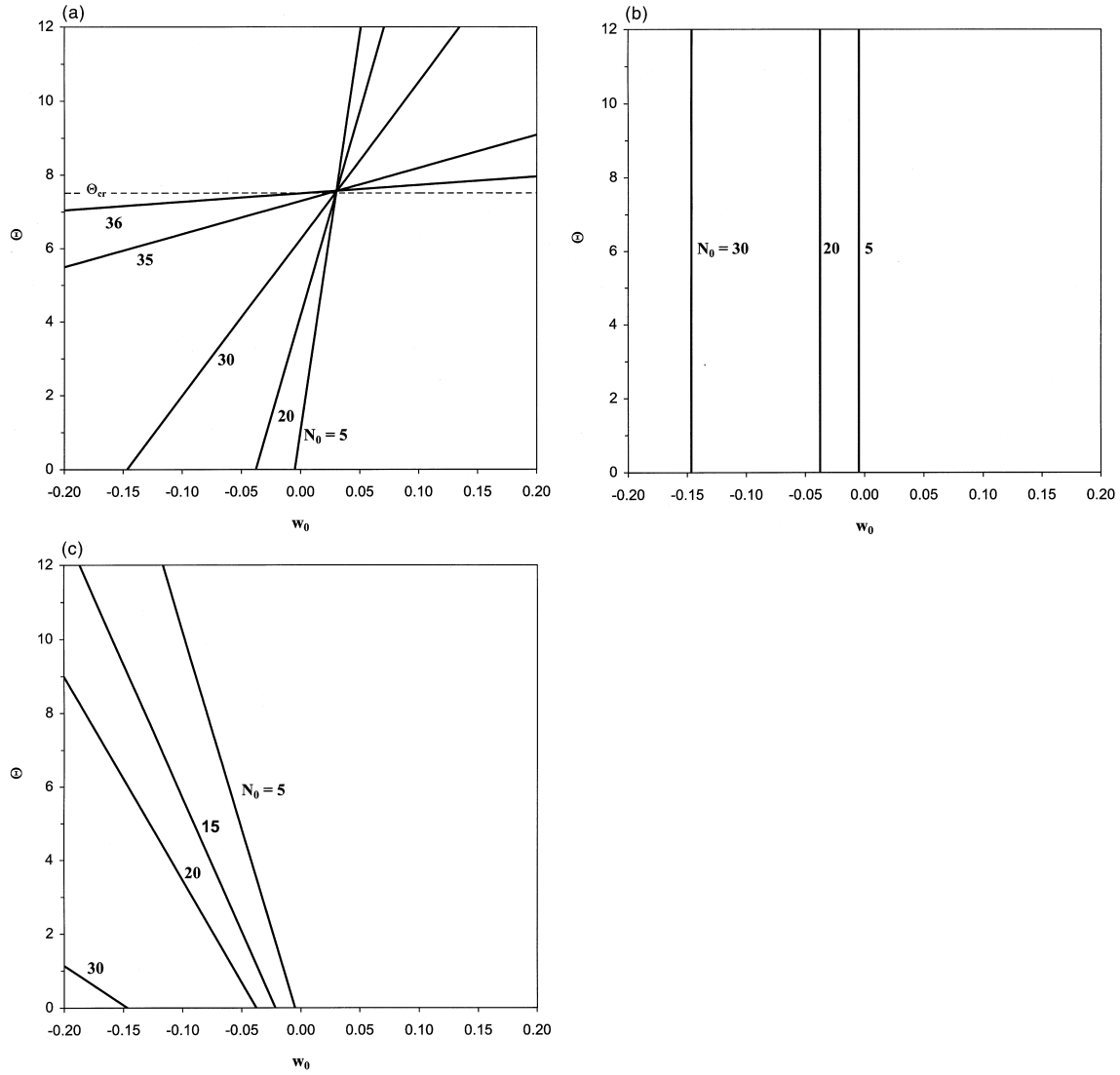

Fig. 6. Normalized temperature, Θ, vs. normalized transverse displacement, w_0, for various values of the normalized membrane force, N_0; (a) $\alpha_0 = 1/2$, (b) $\alpha_0 = 1$, (c) $\alpha_0 = 2$. (*Clamped-Free supports*, $L_p = 0.8$, $E_0 = 1$).

compressive membrane force, N_0, for the ratios of thermal expansion coefficients $\alpha_0 = 1/2$, 1 and 2, respectively. For the case of $\alpha_0 = 1/2$, displayed in Fig. 6(a), it may be seen that for a plate at its reference temperature ($\Theta = 0$), the centerspan deflection is negative (the plate deflects upwards). As the temperature is increased, the deflection eventually becomes positive (downward deflection)[7]. For the case of $\alpha_0 = 1$, it may be seen in Fig. 6(b) that the centerspan deflection is always negative and is independent of

[7] In Fig. 6(a), ($\alpha_0 = 1/2$), all paths appear to cross each other at the critical temperature within the resolution of the figure. This is not actually the case, as would be seen upon magnification in the vicinity of the apparent crossing. Though they appear close, the deflections at $\Theta = \Theta_{cr}$ are not independent of the membrane force.

the temperature, as expected. The response related to a structure where $\alpha_0 = 2$, is displayed in Fig. 6(c). It may be seen that the centerspan deflects upwards, for all applied in-plane edge forces, and increases in magnitude as the temperature increases. In Fig. 6(a,c), it may be seen that the closer the constant membrane force is to the critical membrane force, $N_{cr} = 36.3$, the steeper is the slope of the equilibrium path.

5.1.2. Edges fixed against in-plane translation

We next consider the case where the edges are fixed so as to prohibit in-plane translation and consider temperature controlled loading. We recall that for this case only discrete combinations of membrane forces and temperatures correspond to equilibrium configurations of the structure. Specifically, the membrane force, N_0, is solved numerically as roots to the integrability condition (15), with $u_2(1) = 0$ for each given temperature Θ. We may recall that the in-plane displacements are given in Figs. 2 and 3 for the case of hinged and clamped supports, respectively. For a given temperature the corresponding membrane forces are found where the appropriate isotherm intercepts $u_L = 0$. It may also be noted that there may be multiple membrane forces corresponding to a particular temperature, i.e., there will be more than one possible equilibrium configuration. The issue of which equilibrium configuration the structure will 'prefer' will be discussed shortly. In the following, we limit our discussion to the case of the edges being clamped so as to prohibit rotation. The case of hinged supports, so as to allow edge rotations, shows the same general behavior. Hence, the corresponding results are omitted for brevity.

For the case of clamped edges, it may be seen from Fig. 3 that, for the range of temperatures considered, either one or three equilibrium configurations are possible for a given temperature[8]. In Fig. 7, the associated equilibrium branches are displayed in terms of the thermal and mechanical 'components' of the load parameter, $\mathscr{M}_\lambda$, and the corresponding generalized deflection $\psi = w'(L_p)$ (the rotation at the edge of the patch). Fig. 7(a–c) correspond to $\alpha_0 = 1/2$, 1 and 2, respectively. In each case, the branches are numbered 1, 2, and 3, as indicated in the figures. Branch 1 is associated with the equilibrium path achieved immediately upon loading from the trivial state, branches 2 and 3 are maintained for higher temperatures, where branch number 3 corresponds to the one with highest membrane force. Branches 2 and 3 may be seen to be connected, but we will treat them as separate branches for clarity. It may be noted that for the case of $\alpha_0 = 1$ ($m^* = 0$), all the branches are located in the plane formed by ψ and $(\rho^* + h/2)N_0$.

As more than one equilibrium configuration is possible for a given temperature, it is necessary to establish the stability of each. It may be recalled that according to the criterion set forth in Section 4, an equilibrium configuration is stable if $\mathscr{F} > 0$, where $\mathscr{F}$ is defined by Eq. (37). The function $\mathscr{F}$ is displayed for each branch as a function of the temperature, Θ, in Fig. 8(a–c), for $\alpha_0 = 1/2$, 1 and 2, respectively. Consider first the case of $\alpha_0 = 1/2$, as displayed in Fig. 8(a). It may be seen that, starting at the reference temperature ($\Theta = 0$), only the first branch is present and $\mathscr{F}$ is positive for increasing temperatures for this branch until the critical temperature is reached, at which point, $\mathscr{F}$ becomes negative. In the case of the second branch, it may be seen that $\mathscr{F}$ is negative for temperatures less than the critical temperature, and positive otherwise. Hence, the first branch is stable for temperatures less than the critical temperature and the second branch is stable for temperatures higher than the critical temperature. For other temperatures the branches in question are unstable. The third branch may be seen to be unstable for lower temperatures and stable for higher temperatures, where the switch from unstable to stable is *not* related to the critical temperature. For the cases when $\alpha_0 = 1$ and 2, which are displayed in Fig. 8(b,c), respectively, it may be seen that the first branch is always stable, the second branch is always unstable, and the third branch is unstable for lower temperatures and becomes stable for higher temperatures. In Fig. 9(a–c), the total energy, Π, is displayed, and it may be seen that the

[8] Additional configurations associated with temperatures outside the considered temperature range are possible.

energy is always highest for the third branch, for all α_0. Hence, even within the range where this branch is stable, it is not likely that the associated configurations may be achieved.

With the stability of the equilibrium configurations associated with the various branches established, we now consider the response of the structures of interest during temperature controlled loading. In this context, it is expedient to express the equilibrium paths in terms of the temperature, membrane force and transverse centerspan deflection explicitly. In Fig. 10(a–c), the temperature is displayed as a function of the centerspan deflection, w_0, for $\alpha_0 = 1/2$, 1 and 2, respectively. Consider first the case of $\alpha_0 = 1/2$, as displayed in Fig. 10(a). It may be seen from the figure that the first branch corresponds to negative deflections (upward), while the second and the third branch both correspond to positive deflection (downward). Let us consider a loading scenario for the case where the structure is initially at its reference temperature ($\Theta = 0$) and a monotonically increasing temperature field is subsequently applied. The equilibrium path starts by following the first branch. As Θ is increased, the magnitude of the deflection increases through negative values (becoming increasingly more negative). We may recall that at the point where the critical temperature is achieved the first branch becomes unstable while the second branch becomes stable. Hence, when the surrounding temperature becomes equal to the critical

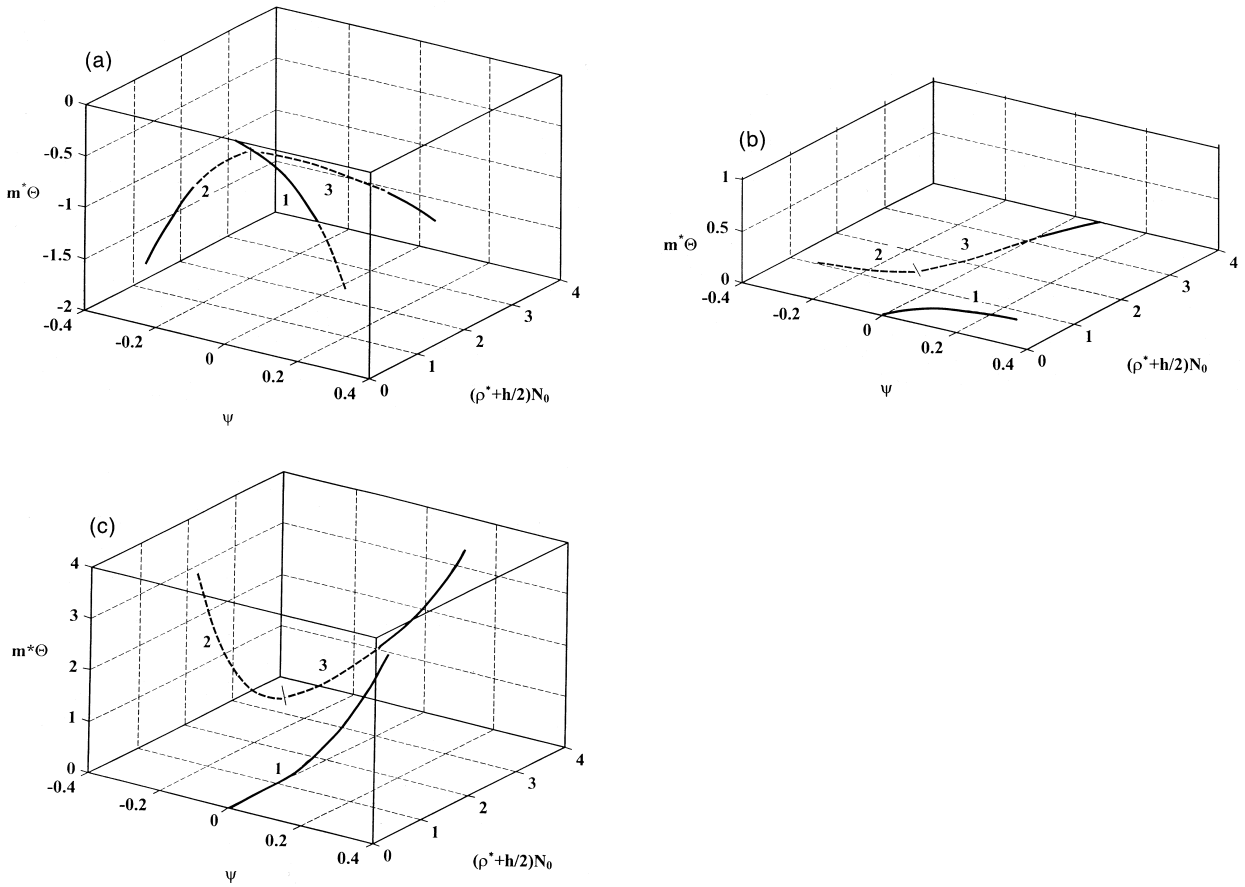

Fig. 7. The first three branches of the equilibrium paths (*Clamped-fixed supports*, $L_p = 0.8$, $E_0 = 1$) displayed in terms of the 'components' of the load parameter, $\mathscr{M}_2$, and the corresponding generalized displacement $\psi = w'(L_p)$; (a) $\alpha_0 = 1/2$, (b) $\alpha_0 = 1$, (c) $\alpha_0 = 2$. (Dashed lines correspond to unstable configurations).

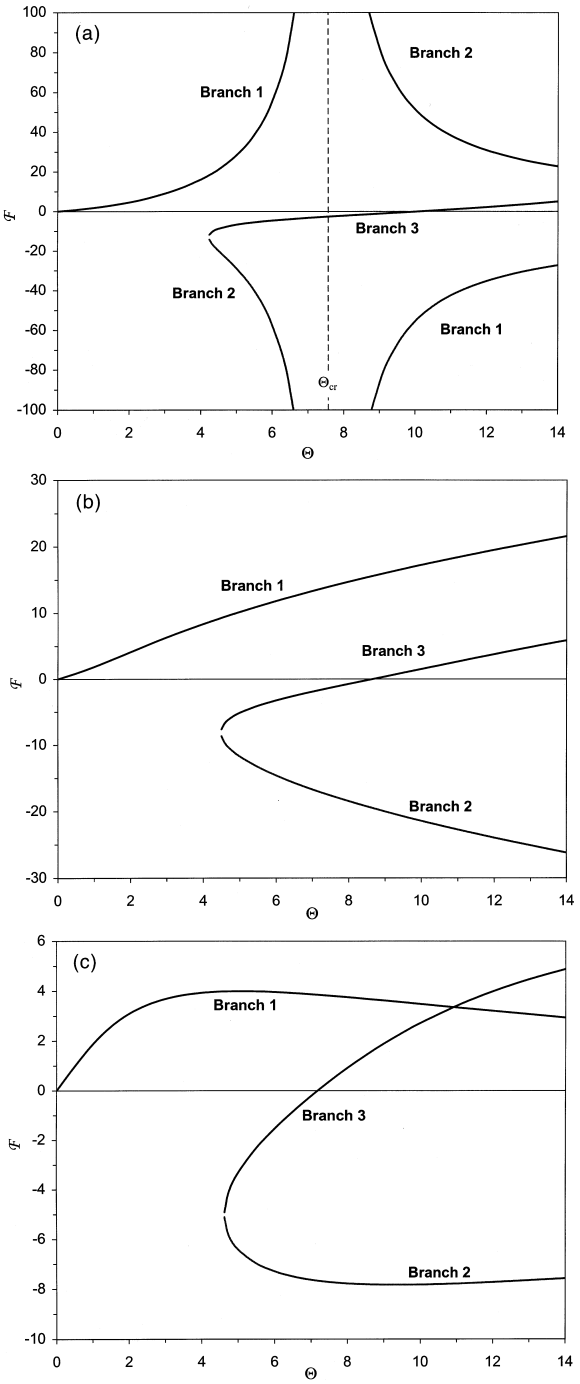

Fig. 8. The stability parameter $\mathcal{F}$ vs. the normalized temperature, Θ, for the first three branches of the equilibrium paths (*Clamped-fixed supports*, $L_p = 0.8$, $E_0 = 1$); (a) $\alpha_0 = 1/2$, (b) $\alpha_0 = 1$, (c) $\alpha_0 = 2$.

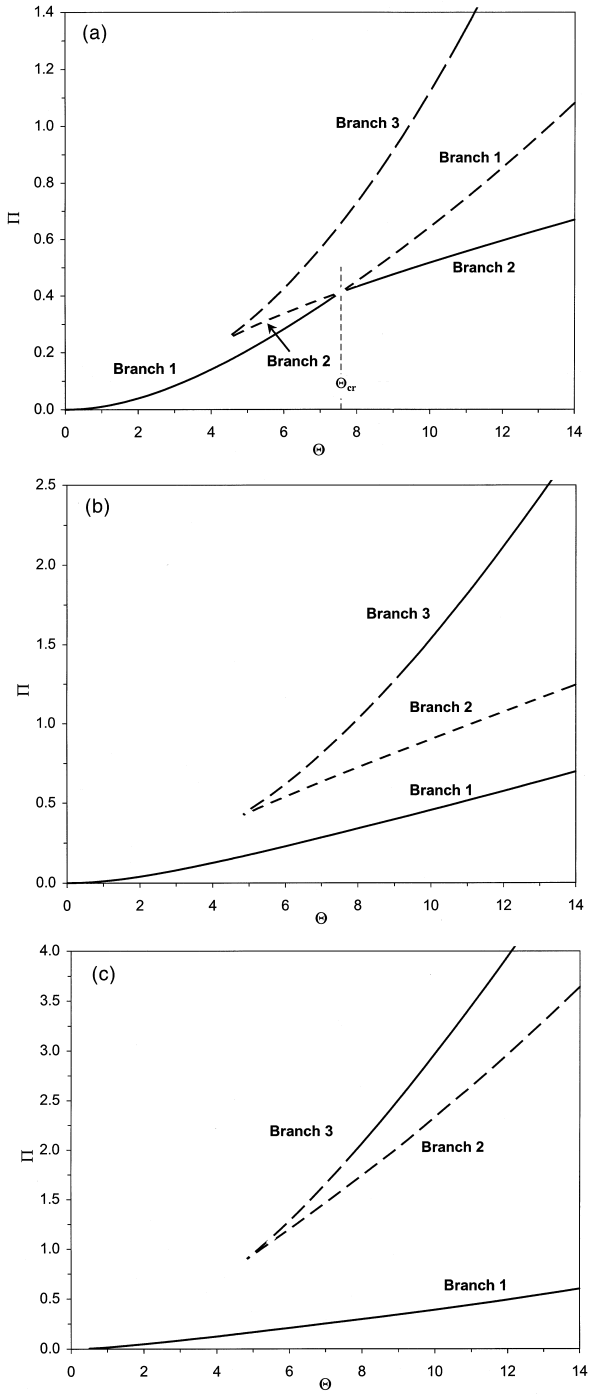

Fig. 9. The total potential energy, Π, vs. the normalized temperature, Θ, for the first three branches of the equilibrium paths (*Clamped-fixed supports*, $L_p = 0.8$, $E_0 = 1$); (a) $\alpha_0 = 1/2$, (b) $\alpha_0 = 1$, (c) $\alpha_0 = 2$. (Dashed lines correspond to unstable configurations).

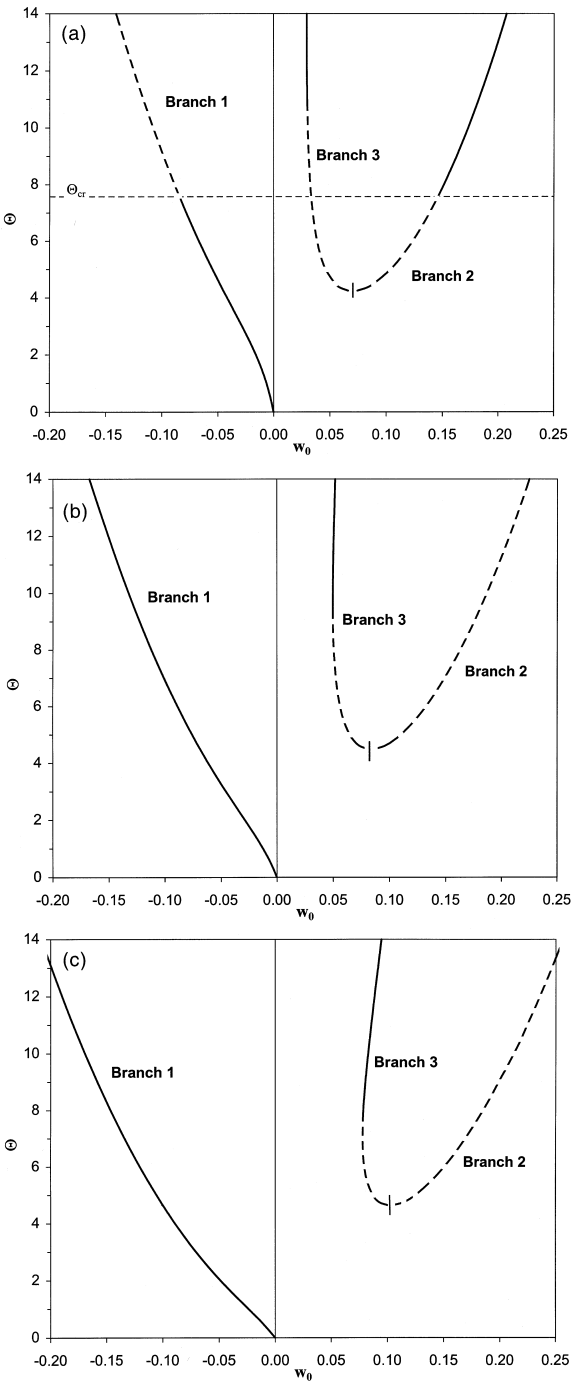

Fig. 10. The normalized temperature, Θ, vs. the normalized transverse displacement, w_0, for the first three branches of the equilibrium paths (*Clamped-fixed supports*, $L_p = 0.8$, $E_0 = 1$); (a) $\alpha_0 = 1/2$, (b) $\alpha_0 = 1$, (c) $\alpha_0 = 2$. (Dashed lines correspond to unstable configurations).

temperature, the transverse deflection of the plate jumps from being negative (deflected upwards) to being positive (deflected downwards). We shall refer to this behavior as 'sling-shot buckling' of the plate[9]. Once the plate has buckled, it continues to deflect downwards with increasing magnitude for increasing temperatures, within the range of temperatures displayed. We next consider the case of unloading, with the following scenario observed: at elevated temperatures ($\Theta > \Theta_{cr}$), the plate will be in a configuration corresponding to the second branch and thus be deflected downwards. Upon cooling, the plate will 'sling-shot' from a downward to an upward deflection, once the critical temperature has been achieved. From this point the centerspan deflection will follow the first branch, down to the reference temperature ($\Theta = 0$). Thus, 'sling-shot buckling' will occur at Θ_{cr}, regardless of whether the critical temperature is reached through increasing or decreasing of the surrounding temperature. For a structure that does not possess a critical positive temperature, such as $\alpha_0 = 1$ and 2, as shown in Fig. 10(b,c), it may be seen that the centerspan deflection will be negative (upwards) for all temperatures studied. Hence, 'sling-shot buckling' does not occur. The behavior just described may be explained in a manner similar to that for the case where the edges of the plate were free for in-plane translations. For this case it was seen that the effects due to temperature and mismatch in coefficients of thermal expansion 'compete' with (for $\alpha < 1$) or reinforce (for $\alpha \geq 1$) effects due to the membrane force.

In Fig. 11(a–c), corresponding to $\alpha_0 = 1/2$, 1 and 2, respectively, the membrane force, N_0, is displayed as a function of the temperature, Θ, for the three branches of equilibrium configurations. Let us first consider the case of $\alpha_0 = 1/2$ [Fig. 11(a)]. It may be seen that at the critical temperature, Θ_{cr}, the first and the second branch correspond to the same membrane force, which is equal to the critical membrane force, N_{cr}. Thus this corresponds to the special case of $\mathscr{M}_\lambda = \mathscr{H} = 0$, as was discussed in Section 3.1. Furthermore, it may be seen that the membrane force will always be less than N_{cr} for the stable solutions. For the cases of $\alpha_0 = 1$ and 2, Fig. 11(b,c), respectively, it may be seen that the second branch always corresponds to a higher membrane force than the first branch, for a given temperature, and that the membrane force of the first branch never exceeds N_{cr}.

5.1.3. Synopsis

The numerical simulations presented above have demonstrated that the critical temperature and the critical membrane force are of great importance to the structural behavior of a patched plate. The critical temperature is related to the existence of bifurcation for the case of an edge-loaded plate with translationally free edges in a constant temperature field or with a constant loading parameter, and to 'sling-shot buckling' for a temperature controlled loaded plate with fixed edges. Furthermore, the critical membrane force is seen to correspond to the structure's 'buckling load'. In the case of in-plane force controlled loading, the membrane force is seen to generally approach, but never exceed the critical membrane force ('asymptotic buckling'), and in the case of 'sling-shot buckling' during temperature controlled loading, the membrane force equals N_{cr} when 'sling-shot buckling' occurs. The qualitative behavior seen for the particular structural parameters considered in this section are characteristic of all structures of this class, within the context of the formulation presented in Section 2. For other patch lengths, structural stiffnesses, and dimensional lengths, variation in critical behavior may be characterized by examination of corresponding variations of the critical temperature and critical membrane force. The behavior of these parameters for various structures is discussed in the next subsection.

[9] We distinguish 'sling-shot buckling' from conventional snap-through buckling since the instability does not occur at a limit load and since the deflection direction is reversed during this process.

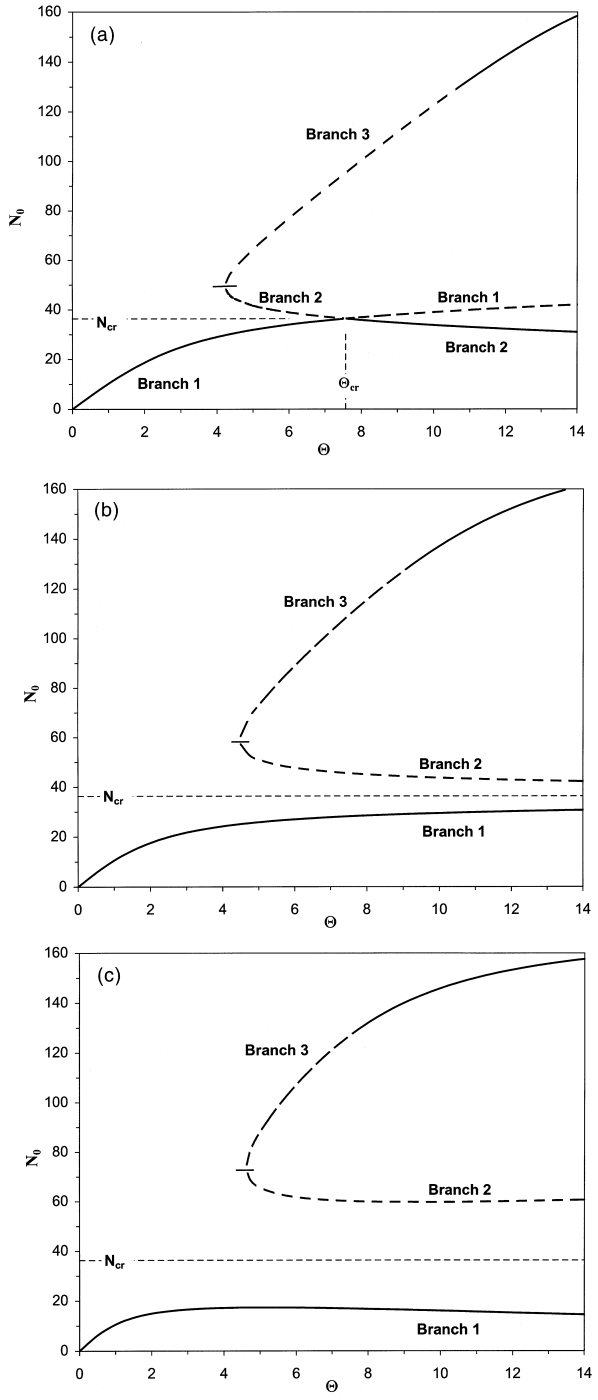

Fig. 11. The normalized (compressive) membrane force, N_0, vs. the normalized temperature, Θ, for the first three branches of the equilibrium paths (*Clamped-fixed supports*, $L_p = 0.8$, $E_0 = 1$); (a) $\alpha_0 = 1/2$, (b) $\alpha_0 = 1$, (c) $\alpha_0 = 2$. (Dashed lines correspond to unstable configurations).

5.2. Critical parameters

In this subsection, the behavior of the two parameters that have been shown above to be of critical importance for the structural response of the patched plate, the critical membrane force, N_{cr}, and the critical temperature, Θ_{cr}, is examined. Both symmetric and antisymmetric deformation is discussed. In particular, the critical force, N_{cr}, and the critical temperature, Θ_{cr}, are presented as functions of the structural properties of the patched plate. These properties include the relative length of the patch, the normalized thickness of the base plate, and the stiffnesses of the composite structure. In each case, the thickness ratio is maintained at unity ($h_p = h$). In order to vary the relative stiffness of the patch, several orders of magnitude of the modulus ratio, E_0, are considered. In this way, the behavior of a broad range of structures is characterized.

We first consider the critical membrane force, the roots of Eq. (25), for symmetric deformations. In Fig. 12, the lowest critical membrane force, N_{cr}, is displayed as a function of the patch length, L_p, for the modulus ratios $E_0 = 0.1$, 1, 10, and thickness $h = 0.05$. Results for hinged supports are shown in

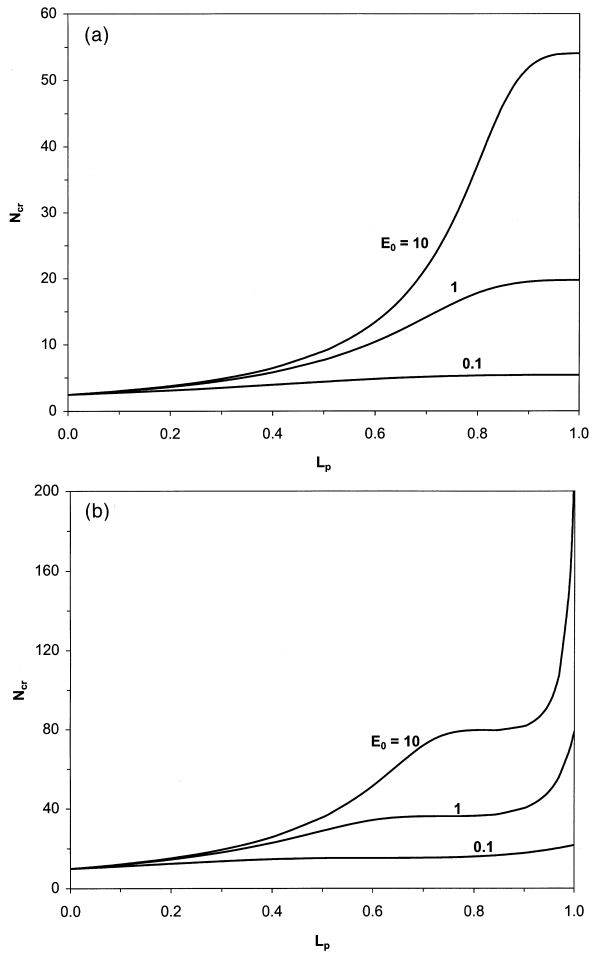

Fig. 12. The first critical membrane force, N_{cr}, for symmetric deformation vs. patch length, L_p, for $E_0 = 0.1$, 1, 10; (a) Hinged support conditions, (b) Clamped support conditions.

Fig. 12(a), while those corresponding to clamped supports, are displayed Fig. 12(b). It may be seen from these figures that the critical membrane force is always larger for the case of clamped supports, and for very long patches ($L_p > 0.95$), the critical membrane force increases significantly over N_{cr} for the hinged case. (We note that the critical normalized membrane force, N_{cr}, is independent of the length of the base plate. It is however related to its dimensional counterpart as in Eq. (4g))

The critical temperature, Θ_{cr}, given by Eq. (26), corresponding to the lowest critical membrane force for symmetric deformation is displayed as a function of α_0 for $\alpha_0 < 1$ in Fig. 13 and 14, for hinged and clamped edge conditions respectively. In Fig. 13(a) and Fig. 14(a), results are shown for various values of the modulus ratio, E_0, for $h = 0.05$. We recall that when $\alpha_0 > 1$, no critical temperature exists. It may be seen that for a given α_0, the critical temperature, Θ_{cr}, increases with increasing stiffness and appears to be asymptotic to the line $\alpha_0 = 1$. Fig. 13(b) and Fig. 14(b) display Θ_{cr} for a range of patch lengths, and it may be seen that Θ_{cr} increases with increasing patch lengths. In Fig. 13(c) and Fig. 14(c), Θ_{cr} is shown for various values of h, where $h_{ref} = 0.05$. It may be seen from these figures that as h increases, the critical temperature increases.

Finally, consider the characteristic parameters associated with antisymmetric deformations. The critical membrane force for this case, $N_{cr_{AS}}$, is given as the roots of Eq. (31), and the critical temperature, Θ_{cr}, is again given by Eq. (26). In Fig. 15(a), the first critical membrane force for both symmetric and antisymmetric deformations is displayed, as a function of the patch length, L_p. Fig. 15(b) shows the critical temperature corresponding to the first critical membrane force for both symmetric and antisymmetric deformations as a function of the ratio of the coefficients of thermal expansion α_0. Both hinged and clamped supports are considered. It may be seen that in all cases, the antisymmetric modes yield significantly higher values of the critical membrane force than do their symmetric counterparts. Thus, if the structure is loaded from the trivial state the antisymmetric load cannot be achieved[10].

6. Concluding Remarks

Thermal buckling of heated patched beam-plates has been investigated. The response of the composite system to a uniform temperature field in combination with a membrane load was described through a self-consistent formulation, yielding a mathematical model of the system in terms of an assemblage of the base structure and the patch. The non-linear problem arising from this formulation was solved analytically, thus results are exact within the context of the formulation. Due to the non-linear nature of the problem, multiple equilibrium configurations are possible and stability of the different equilibrium configurations is an issue. In this regard, a stability criterion was established based on the second variation of the energy potential for the system. Stability of the equilibrium paths was assessed in this context. Various loading and boundary supports were considered.

Several non-dimensional parameters were identified. A loading parameter was determined, consisting of a linear combination of the normalized membrane force and the normalized temperature. All transverse deflections were seen to be proportional to the loading parameter, thus vanishing loading parameter was seen to correspond to flat configurations of the structure. It follows that it is possible to find a loading sequence where the membrane force and temperature is controlled in a manner so that the structure remains flat during increasing temperature for structures where the patch has a lower coefficient of thermal expansion than that of the base plate. Furthermore, two characteristic parameters for the structure were identified, a critical temperature and a critical membrane force. They were seen to characterize the response of the structure.

[10] Unless the system is artificially constrained until the lower N_{cr} is surpassed.

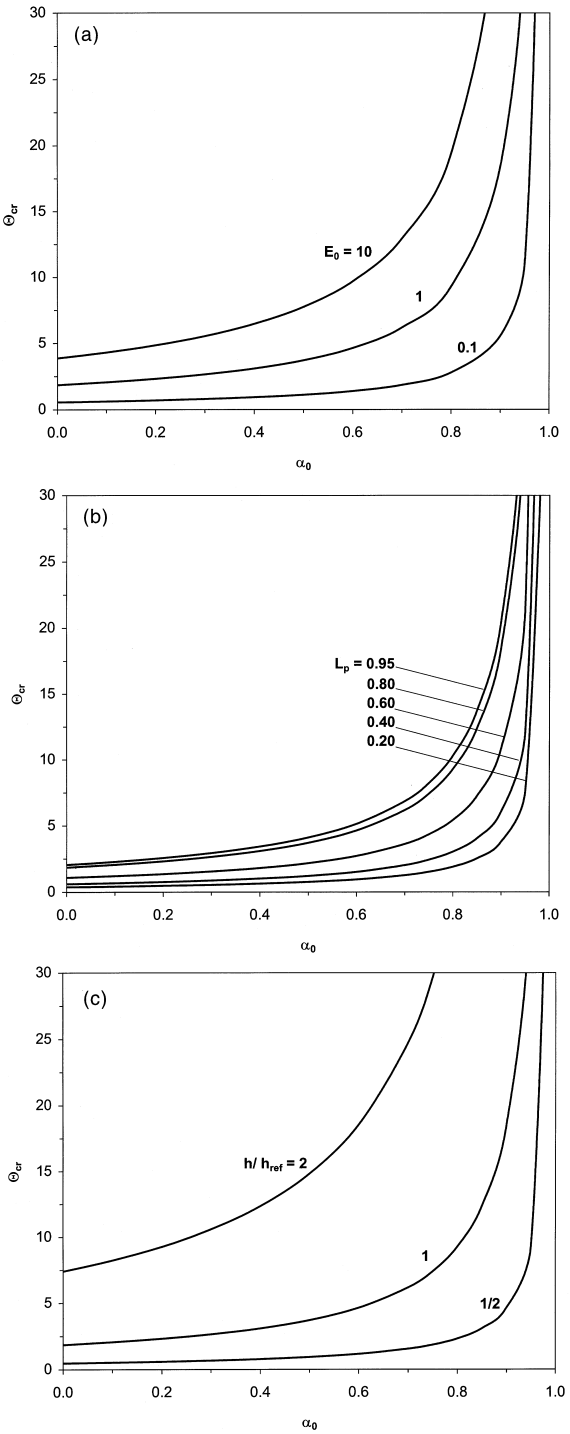

Fig. 13. The critical temperature, Θ_{cr}, corresponding to the first critical membrane force for symmetric deformation vs. the ratio of coefficients of thermal expansion, α_0, for *Hinged supports*; (a) Various relative stiffnesses ($L_p = 0.8$, $h = 0.05$), (b) Various patch lengths ($E_0 = 1$, $h = 0.05$), (c) Various thicknesses, $h_{ref} = 0.05$ ($L_p = 0.8$, $E_0 = 1$).

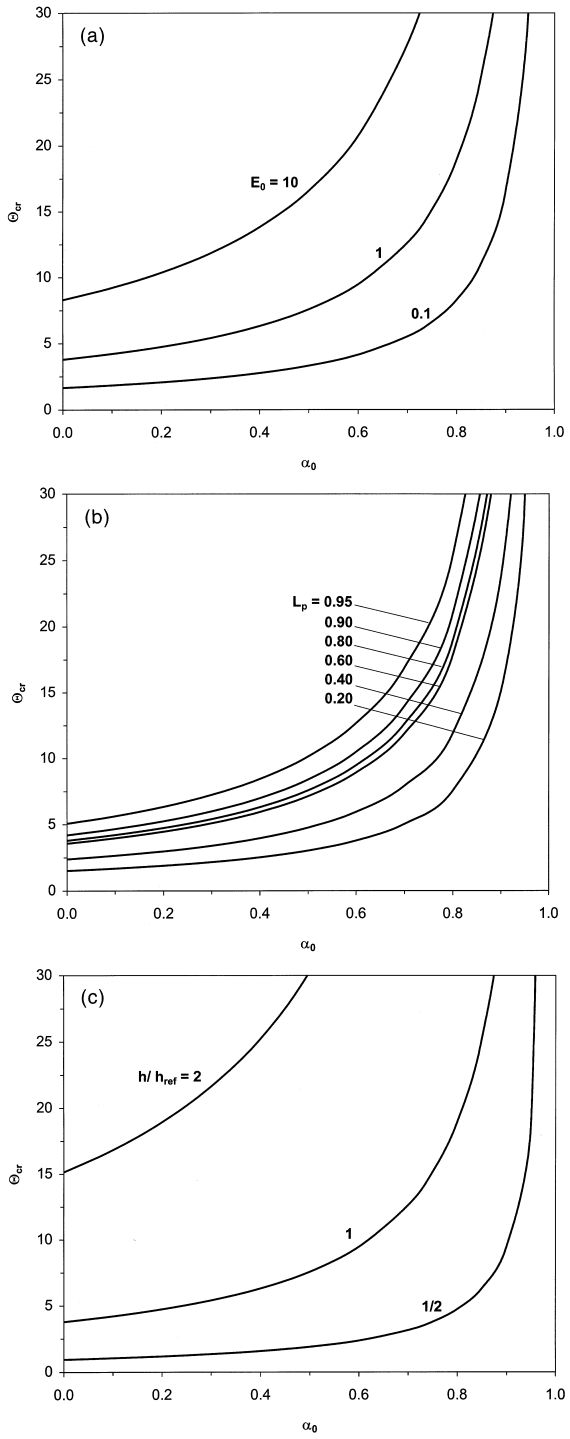

Fig. 14. The critical temperature, Θ_{cr}, corresponding to the first critical membrane force for symmetric deformation vs. the ratio of coefficients of thermal expansion, α_0, for *Clamped supports*; (a) Various relative stiffnesses ($L_p = 0.8$, $h = 0.05$), (b) Various patch lengths ($E_0 = 1$, $h = 0.05$), (c) Various thicknesses, $h_{ref} = 0.05$ ($L_p = 0.8$, $E_0 = 1$).

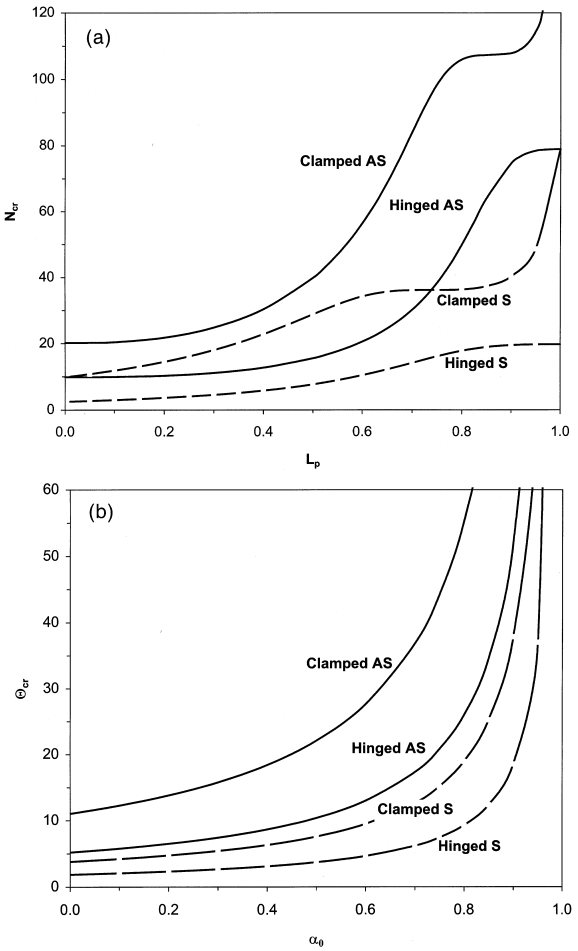

Fig. 15. (a) The first critical membrane force, N_{cr}, vs. patch length, L_p, for symmetric and antisymmetric deformation. ($E_0 = 1$). (b) The critical temperature, Θ_{cr}, corresponding to the first critical membrane force, vs. the ratio of coefficients of thermal expansion, α_0, for symmetric and antisymmetric deformation. ($E_0 = 1$, $L_p = 0.8$).

Results of numerical simulations were presented for representative patched plates to elucidate the characteristic behavior of the class of structures considered, and the results were extended to a broad range of structures by examining the behavior of the characteristic parameters for a variety of geometric and material properties. Three types of critical behavior were observed; bifurcation buckling, 'asymptotic buckling', and 'sling-shot buckling'. The occurrence and characteristics of such behavior were seen to be a function of the critical parameters.

To close, the current investigation of patched beam-plates subjected to thermo-mechanical loading was seen to unveil a rich and varied structural response as well as the factors that control such behavior.

References

Baker, A.A., 1993. Repair efficiency in fatigue-cracked aluminum components reinforced with boron/epoxy patches. Fatigue and Fracture of Engineering Structures 66, 753–765.

Boley, B.A., 1997. Theory of Thermal Stresses. Dover Publication, Mineola, New York, pp. 415–418.
Bottega, W.J., 1995. Separation failure in a class of bonded plates. Composite Structures 30, 253–269.
Bottega, W.J., Karlsson, A.M., 1999. On the detachment of step-tapered doublers: Part 1 — Foundations. Int. J. Solids Structures 36, 1597–1623.
Bottega, W.J., Loia, M.A., 1996. Edge debonding in patched cylindrical panels. Int. J. Solids Structures 33, 3755–3777.
Bottega, W.J., Loia, M.A., 1997. Axisymmetric edge debonding in patched plates. Int. J. Solids Structures 34, 2255–2289.
Dano, M.-L., Hyer, M.W., 1998. Thermally-induced deformation behavior of unsymmetric laminates. Int. J. Solids Structures 35, 2101–2120.
Gauss, R.C., Antman, S.S., 1984. Large thermal buckling of nonuniform beams and plates. Int. J. Solids Structures 20, 979–1000.
Gelfand, I.M., Fomin, S.V., 1963. Calculus of Variations. Prentice–Hall, Englewood Cliffs, New Jersey, pp. 125–129.
Hamamoto, A., Hyer, M.W., 1987. Non-linear temperature–curvature relationships for unsymmetric graphite–epoxy laminates. Int. J. Solids Structures 23, 919–935.
Huang, N.N., Tauchert, T.R., 1988. Postbuckling response of antisymmetric angle-ply laminates to uniform temperature loading. Acta Mechanica 72, 173–183.
Karlsson, A.M., Bottega, W.J., 1999a. The presence on edge contact and its influence on the debonding of patched panels. Int. J. Fracture 96, 383–406.
Karlsson, A.M., Bottega, W.J., 1999b. On the detachment of step-tapered doublers: Part 2 — Evolution of pressure loaded structures. Int. J. Solids Structures 36 (1999), 1625–1651.
Lena, M.R., Klug, J.C., Sun, C.T., 1998. Composite patches as reinforcements and crack arrestors in aircraft structures. J. Aircraft 35, 318–323.
Librescu, L., Souza, M.A., 1993. Post-buckling of geometrically imperfect shear-deformable flat panels under combined thermal and compressive edge loadings. J. Appl. Mech. 60, 526–533.
Naboulsi, S., Mall, S., 1997. Thermal effects on adhesively bonded composite repair of cracked aluminum panels. Theor. & Appl. Frac. Mech. 26, 1–12.
Noor, A.K., Burton, W.S., 1992. Computational models for high-temperature multilayered composite plates and shells. Appl. Mech. Rev. 45, 419–446.
Noor, A.K., Peters, J.M., 1992. Thermomechanical buckling of multilayered composite plates. J. Eng. Mech. 118, 351–366.
Noor, A.K., Starnes Jr., J.H., Peters, J.M., 1993. Thermomechanical buckling and postbuckling of multilayered composite panels. Composite Structures 23, 233–251.
Roderick, G.L. 1980. Prediction of cyclic growth of cracks and debonds on aluminum sheets reinforced with boron/epoxy. In: Lenoe, E.M., Oplinger, D.W., Burke, J.J. (Eds.), Fibrous Composites in Structural Design. Plenum Press, New York, pp. 467–481.
Sih, G.C., Hong, T.B., 1989. Integrity of edge-debonded patch on cracked panel. Theoretical and Applied Fracture Mechanics 12, 121–143.
Simitses, G.J., 1986. An Introduction to the Elastic Stability of Structures. Krieger Publishing Company, Malabar, Florida, pp. 125–127.
Singh, G., Ventkatswara Rao, G., Iyengar, N.G.R., 1993. Thermal post buckling behavior of rectangular antisymmetric cross-ply composite plates. Acta Mechanica 98, 39–50.
Tauchert, T.R., 1991. Thermally induced flexure, buckling, and vibration of plates. Appl. Mech. Rev. 44, 347–360.
Timoshenko, S., 1925. Analysis of bi-metal thermostats. J. Optical Society of America and Review of Scientific Instruments 11, 233–255.
Wahl, A.M., 1944. Analysis of Valverde thermostat. J. Appl. Mech. 11, A183–A189.
Wittrick, W.H., 1953. Stability of a bimetallic disk, Part I. Quart. J. Mechs. and Appl. Math. 6, 15–26.
Wittrick, W.H., Myers, D.M., Blunden, W.R., 1953. Stability of a bimetallic disk, Part II. Quart. J. Mechs. and Appl. Math. 6, 26–31.
Yin, W.-L., 1998. Thermomechanical buckling of delaminated composite laminates. Int. J. Solids Structures 35, 2639–2653.